AD-A092 800 GENERAL ELECTRIC CO SYRACUSE NY MILITARY ELECTRONIC --ETC F/G 20/14
DESIGN OF BROADSIDE ARRAYS USING ITERATIVE INTERPOLATION TECHNI--ETC(U)
SEP 80 J P COSTAS

UNCLASSIFIED R80EMH6 NL

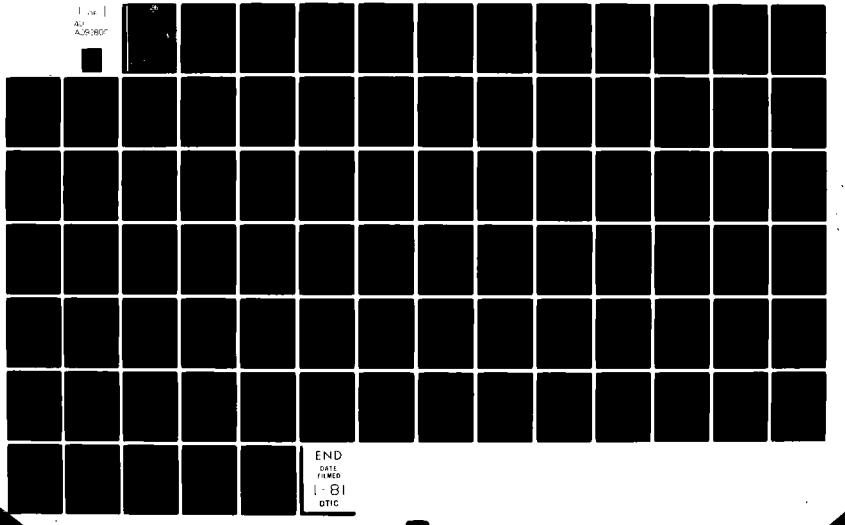

END
DATE FILMED
1-81
DTIC

LEVEL II

(5)

GENERAL ELECTRIC

MILITARY ELECTRONIC SYSTEMS OPERATION

(9) TECHNICAL INFORMATION SERIES

Author	Subject Category	(14) No. R80EMH6
(10) John P. Costas	Antenna Arrays	(11) Date Sept 80

(12) 89

Title (6) DESIGN OF BROADSIDE ARRAYS USING ITERATIVE INTERPOLATION TECHNIQUES.

Copies Available at	GE Class 1	No. of Pages 89
MESO TIS Distribution Center Box 4840 (CSP 4-18) Syracuse, New York 13221	Govt Class Unclassified	

Summary

Arrays having specified beamwidths and sidelobe levels may be synthesized from a simple "seed" array having the required sidelobe level, but a much broader beamwidth than the specification value. An iterative process doubles array spacing at each step. This narrows the main beam by a direct scaling factor of two in sinθ space. The echelon lobes introduced by this action are reduced to the specification sidelobe level values by an interpolation procedure which introduces appropriate element weights at the vacated positions. This "stretch and fill" tactic may be used repeatedly to obtain any beamwidth desired. The computations of weights for these arrays of any size are trivial and the resulting current distributions have a well-behaved taper. Aperture size requirements and efficiencies are consistent with those of conventional designs for a given beamwidth and sidelobe combination. Supergaining problems are not encountered with this procedure.

Interpolation techniques are also used to develop a unique aperture format and excitation matrix combination. This approach to beam steering provides for control of pointing angle through signal level control as opposed to the conventional use of phase shifters for steering.

Send to _____

GENERAL ELECTRIC COMPANY TECHNICAL INFORMATION

Within the limitations imposed by Government data export regulations and security classifications, the availability of General Electric Company technical information is regulated by the following classifications in order to safeguard proprietary information:

CLASS 1: GENERAL INFORMATION

Available to anyone on request.
Patent, legal and commercial review required before issue.

CLASS 2: GENERAL COMPANY INFORMATION

Available to any General Electric Company employee on request.
Available to any General Electric Subsidiary or Licensee subject to existing agreements.
Disclosure outside General Electric Company requires approval of originating component.

CLASS 3: LIMITED AVAILABILITY INFORMATION

Original Distribution to those individuals with specific need for information.
Subsequent Company availability requires originating component approval.
Disclosure outside General Electric Company requires approval of originating component.

CLASS 4: HIGHLY RESTRICTED DISTRIBUTION

Original distribution to those individuals personally responsible for the Company's interests in the subject.
Copies serially numbered, assigned and recorded by name.
Material content, and knowledge of existence, restricted to copy holder.

GOVERNMENT SECURITY CLASSIFICATIONS, when required, take precedence in the handling of the material. Wherever not specifically disallowed, the General Electric classifications should also be included in order to obtain proper handling routines.

GENERAL ELECTRIC COMPANY
MILITARY ELECTRONIC SYSTEMS OPERATIONS
TECHNICAL INFORMATION SERIES

SECTION Advanced Technical Programs

UNIT 570

MESO ACCOUNTING REFERENCE 570

COLLABORATORS

APPROVED J. J. Gostin TITLE Manager, ATP LOCATION CSP 4-58

MINIMUM DISTRIBUTION - Government Unclassified Material (and Title Pages) in G.E. Classes 1, 2, or 3 will be the following.

Copies	Title Page Only	To
0	1	Legal Section, MESO (Syracuse)
0	1	Manager, Technological Planning, MESO (Syracuse)
5	6	G-E Technical Data Center (Schenectady)

MINIMUM DISTRIBUTION - Government Classified Material, Secret or Confidential in G.E. Classes 1, 2, or 3 will be the following.

1	0	Manager, Technological Planning, MESO (Syracuse)

ADDITIONAL DISTRIBUTION (Keep at minimum within intent of assigned G.E. Class.)

COPIES	NAME	LOCATION
5 (CLASS 1 ONLY)	DEFENSE DOCUMENTATION CENTER	CAMERON STATION, ALEXANDRIA, VA. 22314
1	L. I. Chasen	P. O. Box 8555 Philadelphia, Pa., 19101
1	W. B. Adams	CSP 4-48, Syracuse, NY 13221
1	S. P. Applebaum	CSP 4-38A, Syracuse, NY 13221
1	L. W. Bauer	Bldg. 37, Rm. 525, Schenectady, NY
1	T. E. Connolly	CSP 4-57, Syracuse, NY 13221
1	F. R. Dickey, Jr.	CSP 4-38A, Syracuse, NY 13221
1	M. D. Egtvedt	CSP 5-1H, Syracuse, NY 13221
1	B. H. Geyer, Jr.	CSP 5-6G, Syracuse, NY 13221
1	J. J. Gostin	CSP 4-58, Syracuse, NY 13221
1	R. V. Jackson	CSP 4-5, Syracuse, NY 13221
1	M. A. Johnson	CSP 4-58, Syracuse, NY 13221
1	D. T. Hurley	MD 310, French Rd, Utica, NY
1	T. G. Kincaid	Bldg. 37, Rm. 523, Schenectady, NY
1	R. R. Kinsey	CSP 4-57, Syracuse, NY 13221
1	D. R. Morgan	EP 3-234, Syracuse, NY 13221
1	C. E. Nelson	CSP 4-38A, Syracuse, NY 13221
1	E. Niemann	U4424, P. O. Box 8555 Philadelphia, Pa., 19101
1	R. Nitzberg	CSP 4-5, Syracuse, NY 13221
1	G. Oehling	CSP 4-5, Syracuse, NY 13221
1	G. A. Otteni	CSP 4-57, Syracuse, NY 13221
1	D. W. Perkins	CSP 5-2T, Syracuse, NY 13221

Additional Distribution (Cont)

Copies	Name	Location
1	C. M. Puchette	Bldg. 37, Rm. 449, Schenectady, NY
1	H. Scudder	Bldg. 5, Rm. 209, Schenectady, NY
1	F. D. Shapiro	CSP 4-5, Syracuse, NY 13221
1	T. B. Shields	CSP 5-7K, Syracuse, NY 13221
1	J. F. Slocum	CSP 4-4, Syracuse, NY 13221
1	C. A. Stutt	Bldg. 5, Rm. 209, Schenectady, NY
1	B. W. Tietjen	FRP 1-1N, Syracuse, NY 13221
1	H. Q. Totten	CSP 5-2E, Syracuse, NY 13221
1	B. P. Viglietta	CSP 4-57, Syracuse, NY 13221
1	A. H. Vural	CSP 4-48, Syracuse, NY 13221
1	W. P. Whyland	CSP 4-48, Syracuse, NY 13221

TABLE OF CONTENTS

LIST OF ILLUSTRATIONS

LIST OF ILLUSTRATIONS (Cont)

SECTION I

BACKGROUND

Since the work presented here draws heavily upon some previous interpolation studies by the writer [1] , a cursory review of this material will be presented. A sampled-data (time-quantized) time series is considered which involves a sampling period T, and a corresponding sampling rate R (R = 1/T). The power density spectrum of the continuous (but unavailable) time function originally sampled is assumed to be band limited with a cutoff frequency which is no greater that the foldover frequency (R/2) of the sampling process. It is desired to raise the sampling rate to some higher value by some efficient means. That is, it is desired to estimate the sample values of the continuous time series which lie between the available values which are delivered to the processor at T-second intervals. The estimation errors are to be minimized (in some sense) for a given data processing cost.

The procedure employed is one in which the sampling rate is doubled at each of a number of levels using processors of the type shown in Figure 1-1. Time samples of the continuous function s(t) enter a tapped delay line, and the weighted sum of the 2N samples is used as the estimate of the intermediate value between each input sample pair. The original input samples are recovered at the a_{-1}, tap, delayed one-half the input sampling period, and merged with the intermediate estimates from the summing bus. The output sampled-data stream would consequently have a period of T/2 and a sampling rate 2R. It is thus argued that if these intermediate value estimates are the best that can be obtained from the original input data, then these estimates should be used if further sampling rate multiplications (additional intermediate estimates) are desired. A cascade of processors of the type shown in Figure 1-1 are indicated with sampling-rate doubling occurring at each level or stage.

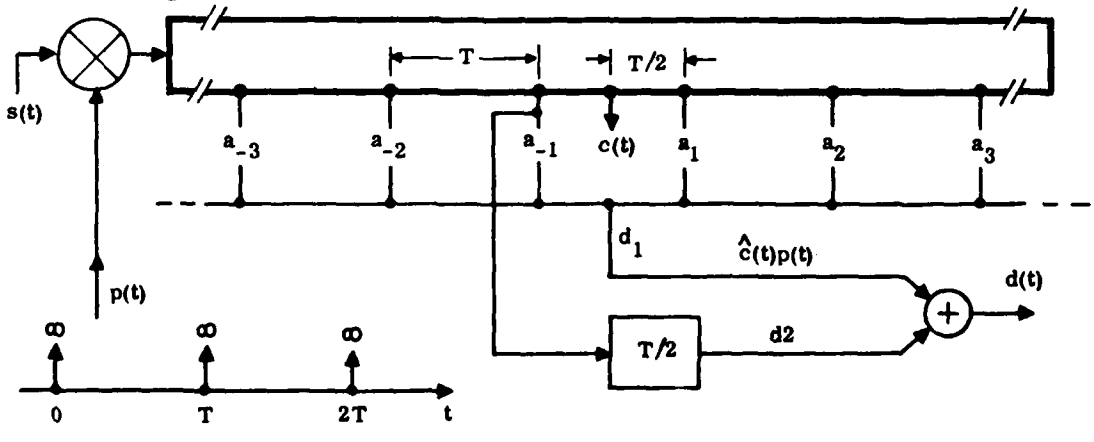

Figure 1-1. Interpolation Processor, Sampled Data Version

The above process is efficient in that processing results obtained from previous levels are available for use in levels following. The interpolator design at each level can be tailored to meet the needs at that level. As the sampling rate is increased through the cascade the interpolation task becomes easier since the available input samples are closer to, and hence more strongly correlated with, the intermediate values to be estimated. Early in the cascade, where the sampling rate is low, one finds the the most complex (longest) interpolation processors. The simplest (shortest) interpolation processors are found at the end of the iterative interpolation chain where the sampling rate is highest. Rate multiplication factors that are not powers of two may be obtained by easily-configured multiplication/resampling procedures [1, Section 5.4] .

The performance of the processor of Figure 1-1 may be evaluated by a frequency-domain technique [1, Section 2.3] which leads, concurrently, to a method for determining the processor coefficients of Figure 1-1. If the input signal s(t) has a low-pass spectrum which extends to the foldover frequency R/2, the spectrum of the input sampled-data series will contain upper and lower sideband terms of total bandwidth R located about suppressed (AM) carriers centered at positive and negative multiples of the input sampling rate R. If a perfect interpolation could be achieved, the output spectrum would be identical to the input spectrum except that frequency groups at odd multiples of R would be missing, and the groups at even multiples of R would represent a doubling of (voltage) level. This result follows since perfect interpolation would be equivalent to use of a sampling rate of 2R on the original s(t) data.

The interpolation portion of Figure 1-1 should have an effective (relative) frequency response (real, even) function which is exactly one for $0 \leq f \leq R/2$ and is minus one from $R/2 \leq f \leq R/2$. A good design approach [1, Section II] employs a symmetric processor of total length 2N. That is, for Figure 1-1

$$a_n = a_{-n} \tag{1-1}$$

so define

$$b_n = 2a_n \tag{1-2}$$

which yields the real frequency function H (f),

$$H(f) = \sum_{n=1}^{N} b_n \cos (2n-1)\, \pi \, \frac{f}{R} \tag{1-3}$$

Note that

$$H(f+2R) = H(f) = -H(f+R) \tag{1-4}$$

so that the unity specification about f = 0 automatically accomodates the -1 specification about f = R.

Since the ideal H(f) behavior is unreachable, one may define a frequency limit γ R/2 and a magnitude tolerance δ which require N and b_n choices so that

$$| 1-H(f) | \leq \delta \text{ for } 0 \leq f \leq \gamma R/2 \tag{1-5}$$

The γ term defines a passband over which good interpolation is achieved and the δ term controls the quality level of the interpolation. The passband ripple of the processor (usually not a problem) is controlled by δ as is the stopband attenuation (usually controlling) about f = R. As expected, interpolator complexity (N value of Equation (1-3) increases with increasing γ and decreasing δ. In later portions of this paper interpolation processors will be used [1, Section VI] which will be referenced by a type value NT. Type selection implies a particular (γ, δ) pair where the δ value is usually indicated in terms of stopband attenuation level. An interesting class of digital filters may be obtained [1, Section IV] from the impulse response of the interpolation cascade. (H(f) of Equation (1-3) has an elliptic filter behavior [2, Section 4.9] .)

The well-known duals between discrete time series and line arrays may be documented for convenient reference with the aid of Figure 1-2. The frequency-domain description of the discrete time series of Figure 1-2a may be obtained from the Discrete Fourier Transform

$$X(f) = \sum_k x_k \, e^{-j 2\pi k \frac{f}{R}} \tag{1-6}$$

where

$$X(f+R) = X(f) \tag{1-7}$$

so that quantization (sampling) in the time domain leads to a periodicity in the frequency domain.

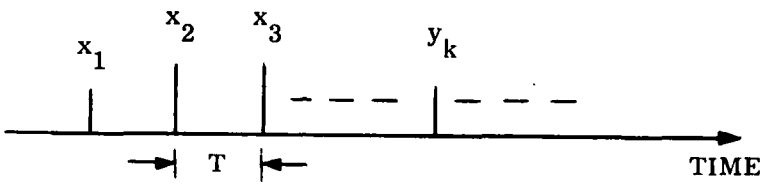

a) Discrete Time Series

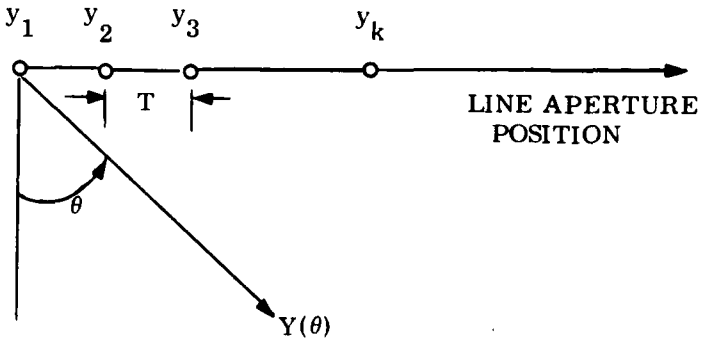

b) Line Array Geometry

Figure 1-2. Time Series and Line Array Geometry

If the symbol T is also used to represent element spacing for the line array of Figure 1-2b, the far-field pattern $Y(\theta)$ will be given by

$$Y(\theta) = \sum_k y_k \, e^{+j 2\pi k \frac{\sin\theta}{(\lambda/T)}} \tag{1-8}$$

In a sense (λ/T) represents a sampling rate since this ratio equals the number of array elements per wavelength. So if for Equation (1-8) we define

$$f = \sin\theta \tag{1-9}$$

and

$$R = \lambda/T \tag{1-10}$$

We obtain

$$Y(f) = \sum_k y_k \, e^{+j 2\pi k \frac{f}{R}} \tag{1-11}$$

where

$$Y(f + R) \quad Y(f) \tag{1-12}$$

which reveals that sampling in the aperture domain leads to periodicity in the far field domain ($\sin\theta$ space).

While there is only a trivial sign difference between Equations (1-6) and 1-11), there are physical differences in the situations of origin which should be kept in mind. In the array case f values outside the ±1 range do not represent physical pointing angles, of course, even though all f values are mathematically acceptable. The selection of element spacing (R determination) is a complicated function of many engineering considerations such as mechanical design, maximum scan angle, element mutual coupling effects, etc. These factors vary considerably from one application to another. It will be assumed here that R for the line array is prespecified by the application and must be maintained in the final design. It should be noted from Equation (1-11) that the far-field pattern in $\sin\theta$ space is directly scaled by varying the element spacing.

In the next section interpolation techniques are used to restore the sampling rate to the prespecified R value after a previous operation doubled the spacing in order to reduce the $\sin\theta$ beamwidth by a factor of two. Thus interpolation is used to fill voids in a stretched

array. This procedure achieves desired beamwidth and sidelobe level specifications by a careful insertion of new elements into a starting "seed" array which is repeatedly stretched and filled. Since R is maintained, the aperture size is expanded by the process.

SECTION II

INTERPOLATION CONCEPT

The pattern synthesis technique to be described uses mathematical procedures which are based on interpolation methods previously discussed. While the mathematics and the responsive algorithms may be described in a unique fashion, there are two physical interpretations of the process which justify separate expositions. The interpolation concept follows the philosophy of the previous section directly, and will be presented first. The "Auxiliary Array" concept discussed later involves a much different interpretation which represents a useful alternate physical justification of the design procedure.

Let a beamwidth (unless otherwise stated -3 dB values are implied) and sidelobe peak level be specified for an array for a given element spacing or R value. We select a starting or "seed" array which has the requisite sidelobe level but (generally) has a much larger beamwidth than that desired. The choice of seed is not critical, it is only required that a contiguous sidelobe region exist whose peak level is no larger than that specified for the final array. A convenient seed for many applications may be represented by a Chebyshev design as discussed by Dolph and others [3,4] .

The seed is shown in Figure 2-1(a) with the (prespecified) element spacing T which yields the required R value (λ/T). The element weights are indicated by the s_k terms. The pattern for the seed is sketched in Figure 2-1(c) having a sidelobe region which begins at $\gamma R/2$ in sin θ (f) space. The seed pattern is periodic with periods equal to the sampling rate R as indicated in the $S_T(f)$ sketch. We now stretch the seed array spacing to 2T as indicated by the s_k element terms of Figure 2-1(b). The far-field pattern of the stretched seed array will be scaled 2:1 in f-space with a new sampling rate of (R/2) as indicated by the $S_{2T}(f)$ plot in Figure 2-1(d). Comparing $S_{2T}(f)$ with $S_T(f)$ in Figure 2-1 it is seen that from an absolute f-scale viewpoint, the stretching has narrowed the main beam which is desired, but an "echelon" lobe has been introduced at f = R/2 which cannot be tolerated. The problem, therefore, is one of using the interpolation processor portion of Figure 1-1 to produce a new set of weights τ_k. These weights will be placed on 2T centers and interleaved with the s_k set as shown in Figure 2-1(b). By this aperture interpolation process we hope to eliminate the "echelon lobe" at f = R/2 in the $S_{2T}(f)$ function, and restore the aperture sampling rate to the prespecified R-value. Note that the interpolation sequence τ_k has the same element spacing as the "input" or "source" array, but is introduced with an aperture position offset of half the "input" element spacing, (2T)/2 = T. The comparisons with the time series interpolation (sampling rate multiplication) process of Section I are easy to make.

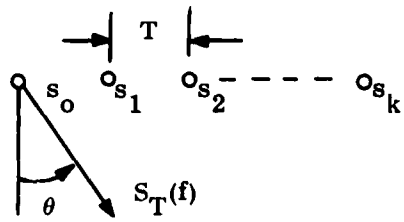

a) Original "Seed" Array

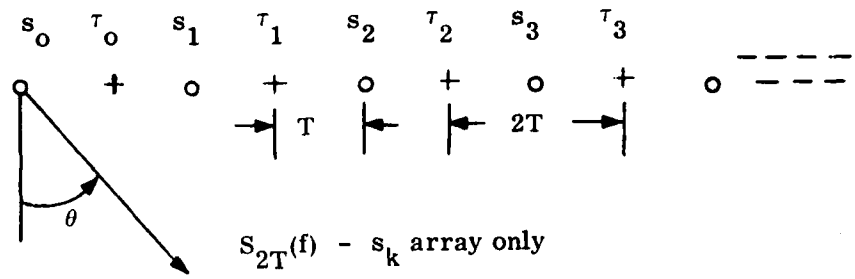

$S_{2T}(f)$ - s_k array only

$E_{2T}(f)$ - τ_k array only

$S'_T(f)$ - s_k and τ_k array

b) Stretched Seed With Interpolation Array Interleaved

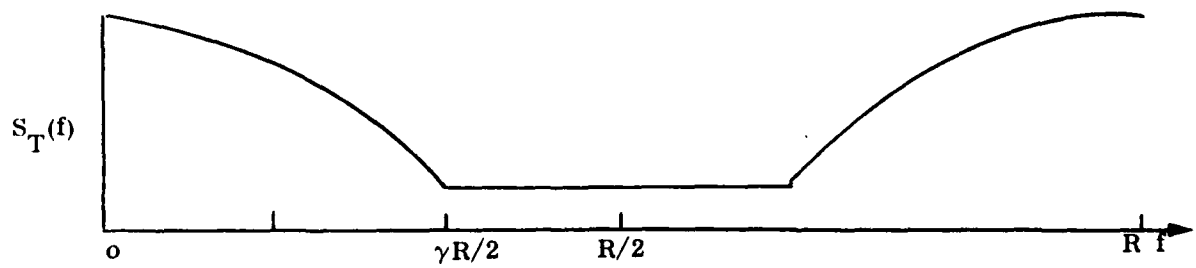

c) Seed Array Far-Field Pattern

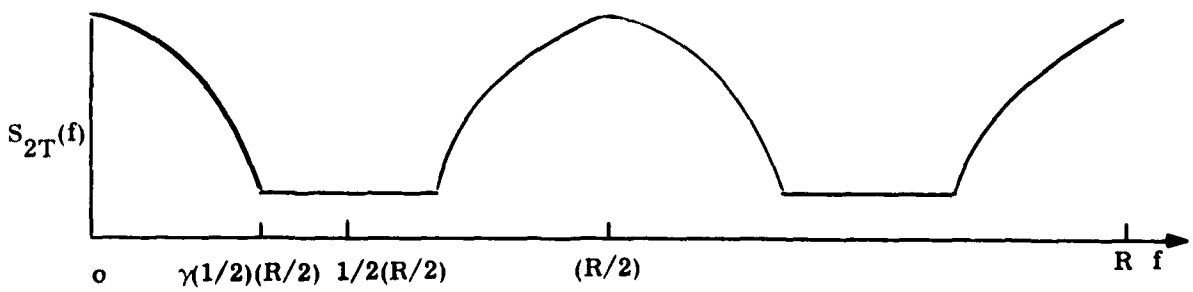

d) Far-Field Pattern of Stretched Seed Array

Figure 2-1. Interpolation Concept Sketches (Sheet 1 of 2)

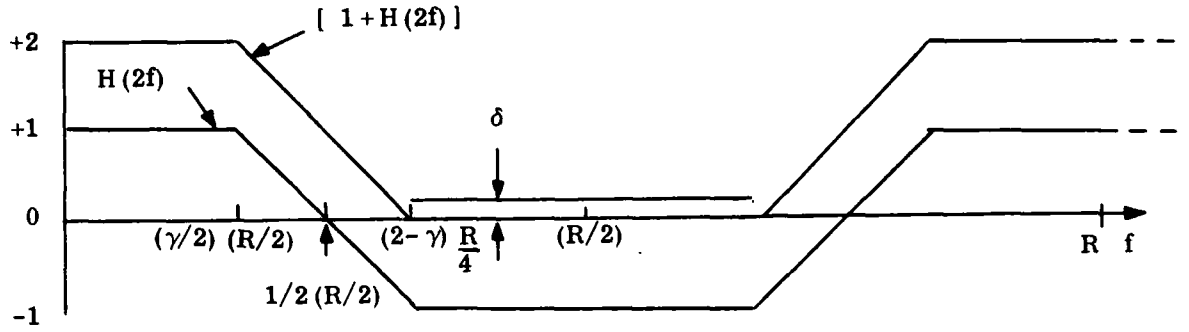

e) H(2f), [1+H(2f)] Behavior

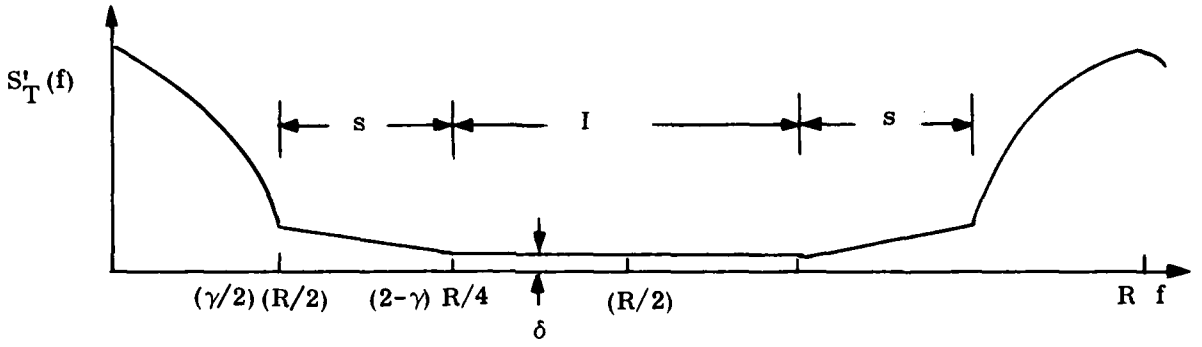

f) Final Output Pattern From First Processing Level

Figure 2-1. Interpolation Concept Sketches (Sheet 2 of 2)

Consider now a method for generating the τ_k weights from the s_k weights. The far-field pattern of the original seed is given by Figure 2-1(a).

$$S_T(f) = \sum_k s_k \, e^{+j\,2\pi k \frac{f}{R}} \tag{2-1}$$

where, as before

$$f = \sin\theta \tag{2-2}$$

$$R = \lambda/T \, . \tag{2-3}$$

The pattern for the stretched seed is

$$S_{2T}(f) = \sum_k s_k e^{+j\,2\pi k \frac{f}{(R/2)}} \tag{2-4}$$

which simply says that

$$S_{2T}(f) = S_T(2f) \, . \tag{2-5}$$

It follows at once from Equation (2-4) and Figure 2-1(b) that the far-field pattern of the τ_k array is given by

$$E_{2T}(f) = \sum_k \tau_k \, e^{+j\,2\pi (k+1/2) \frac{f}{(R/2)}} \, . \tag{2-6}$$

If the input seed values s_k are entered sequentially into the interpolation processor of Figure 1-1 they will appear in the delay element in reverse order with the lowest index values to the right (convolution effect). Keeping this and the indexing used in Figure 2-1(b) in mind, the interpolation weights τ_k may be obtained from

$$\tau_k = \sum_{n=1}^{N} \left(a_{-n} \, s_{k+n} + a_n \, s_{k+1-n} \right) . \tag{2-7}$$

Since a symmetric processor is to be used

$$a_n = a_{-n} \tag{2-8}$$

allows Equation (2-7) to be simplified as

$$\tau_k = \sum_{n=1}^{N} a_n \left(s_{k+n} + s_{k+1-n} \right) . \tag{2-9}$$

Substitute Equation (2-9) into Equation (2-6)

$$E_{2T}(f) = \sum_k e^{+j2\pi(k+1/2)\frac{f}{(R/2)}} \sum_{n=1}^{N} a_n \left(s_{k+n} + s_{k+1-n} \right) . \tag{2-10}$$

Now interchange the order of summation to get

$$E_{2T}(f) = \sum_{n=1}^{N} a_n \left[\sum_k e^{+j2\pi(k+1/2)\frac{f}{(R/2)}} s_{k+n} + \sum_k e^{j2\pi(k+1/2)\frac{f}{(R/2)}} s_{k+1-n} \right] \tag{2-11}$$

Replace k by k-n in the first interior sum and by k+n-1 in the second interior sum to yield:

$$E_{2T}(f) = \sum_{n=1}^{N} a_n \left[e^{-j\pi(2n-1)\frac{f}{(R/2)}} \sum_k s_k e^{+j2\pi k\frac{f}{(R/2)}} + e^{j\pi(2n-1)\frac{f}{(R/2)}} \sum_k s_k e^{+j2\pi k\frac{f}{(R/2)}} \right] . \tag{2-12}$$

Substitution of Equation (2-4) simplifies to

$$E_{2T}(f) = S_{2T}(f) \sum_{n=1}^{N} b_n \cos(2n-1)\frac{\pi f}{(R/2)} \tag{2-13}$$

where

$$b_n = 2a_n \tag{2-14}$$

as before. Equation (1-3) permits further simplification to

$$E_{2T}(f) = S_{2T}(f)\, H(2f) \ . \qquad (2\text{-}15)$$

When the stretched seed and the interpolated array are merged (Figure 2-1(b)), the resultant pattern is

$$S'_T(f) = S_{2T}(f) + E_{2T}(f) = S_{2T}(f)[\, 1+H(2f)] \ . \qquad (2\text{-}16)$$

From the discussion in Section I the behavior of H(2f) and [1+H(2f)] is sketched in Figure 2-1(e). H(2f) remains near unity out to $\gamma R/4$ then follows a transition region from $\gamma R/4$ to $(2-\gamma) R/4$. At this f value the -1 region about f = R/2 begins.

The [1+H(2f)] factor starts at a level of two. At the center of the transition region (R/4) the value is one (6-dB down from peak response). The "stopband" region begins at $(2-\gamma)$ (R/4) with a peak voltage gain of δ. Note that the direct δ suppression value in decibels must be increased by 6 dB to account for the voltage gain of two in the "pass" region of [1+H(2f)] .

The final output far-field pattern of the merged array is obtained by taking the product $S_{2T}(f)$ of Figure 2-1(d) with the [1+H(2f)] factor of Figure 2-1(e). The result for $S'_T(f)$ is sketched in Figure 2-1(f). The echelon lobe of $S_{2T}(f)$ at R/2 has been reduced by the process, and the pattern period is again R as required. The new sidelobe regions of $S'_T(f)$ may be identified as originating (mainly) from the seed or from the interpolation process. These regions are so identified in Figure 2-1(f) by the "s" and "I" designations.

In Figure 2-1(f) δ is shown at a lower level than the seed sidelobe level for delineation purposes only. Normally these two sidelobe levels are matched in design. In spite of this, sidelobe peak levels only are directly controlled, with sidelobe peaks normally occurring near the edge of the main beam or near R/2. Sidelobes elsewhere normally drift to lower levels, which are sometimes brought back to the design value by an aperture truncation process to be described later.

One can now logically accept the merged array of Figure 2-1(b) as a new "seed" and repeat the whole process to obtain further mainlobe frequency scaling. The basic concept can be extended to any number of levels. In fact, the interpolator design becomes simpler at the later levels. Note in Figure 2-1(f), for example, that the γ value operative here is one-half that encountered in the true seed. Hence, it follows from the discussion of Figure 1-1 that interpolator design becomes simpler at each succeeding level because the design γ is cut in half even though the δ specification is maintained.

(The exceptionto this occurs for those cases in which the main beam extends beyond the interpolator $\gamma R/2$ at the seed level. This will often result in an unacceptable sidelobe peak to the left of $(2-\gamma)R/4$ in Figure 2-1(f). A second level γ larger than the normal half-value will be needed to clear this up [1, Section 3.2] . After this special "extended-gamma" second level, the usual half-gamma sequence may be followed in the remainder of the cascade.)

In the multilevel aperture synthesis procedure the output at each level contains all of the elements of the preceding level in addition to the new interpolated elements generated at that level. The new elements are generated entirely from excitation values that inhabit the previous level. There is never any "reaching back" in the drive matrix beyond the immediate level. An element once created at a level appears at all succeeding levels, including the final one. This, if one looks carefully at a multilevel synthesis result, the original seed will always be found. Note also that the operation which processes 2N excitation values from a previous level (Equation 2-9) to produce an interpolated value for the next level is invariant with element location at that level. The design changes from level to level, but the same design is used at all element positions within a given level.

Consider now an alternate use of the interpolation concept. Let the seed array of Figure 2-2(a) be of some desired ultimate design which has the appropriate beamwidth, sidelobe levels, and element spacing. Now let it be required that a second array, physically interleaved with the first, and having the same element spacing, T, as the seed array be created so that its far-field pattern matches that of the seed within a specified tolerance over a specified region of the far field. (A practical need for this "array substitution" function was recently brought to the writer's attention.)

The problem now becomes one of deriving a set of element weights τ_k from the given set s_k so that the far-field pattern of the τ_k array, $E_T(f)$, matches the far-field pattern, $S_T(f)$ of the s_k array. If the logic which led from Equation (2-1) to Equation (2-15) is followed without the doubling of T, one obtains in a routine manner the result

$$E_T(f) = H(f)\, S_T(f) \qquad (2\text{-}17)$$

where H(f) is defined by Equation (1-3) as before and Equations (2-7) and (2-9) are valid without alteration.

If the τ_k currents are derived from the s_k current set via the matrix represented by Equation (2-9), the far-field of the τ_k array will be identical to that of the s_k field except for a possible level error as indicated in Figure 2-2(b). The gain error remains small out to a "cut off" far-field angle which correponds to $\gamma R/2$. (This is essentially a limit on the

amount of beam steering that may be done.) The closeness of the gain match in the operating region (δ) is a function of interpolator choice as is the γ value.

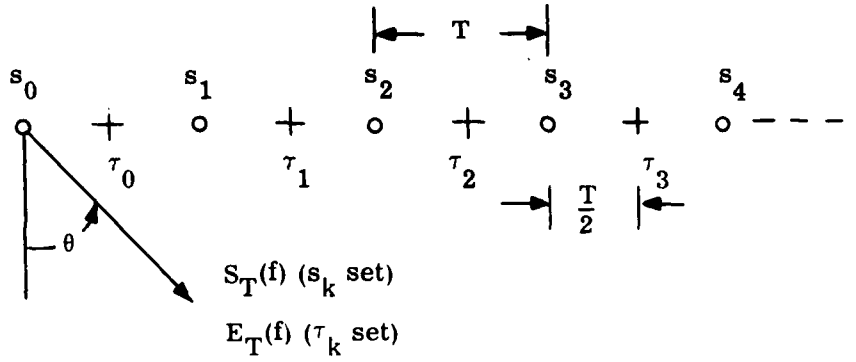

(a) Interleaved Array Geometry

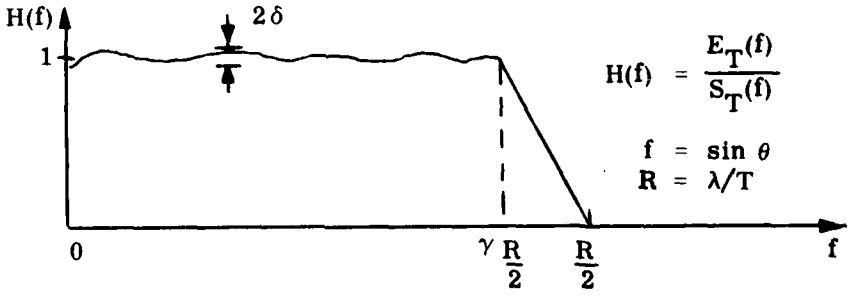

(b) Interleaved Array (τ_k set) Far-Field Response Function

Figure 2-2. Displaced Array Substitution

Determination of the τ_k weights may be done very easily using the techniques of this paper. One merely inputs the s_k sequence into the appropriately selected interpolation subroutine as described in Section IV and the interleaved (s_k, τ_k) set of Figure 2-2(a) will automatically be generated by the program. Additional τ-elements with intervening zero-weight s-elements will automatically be added at the array ends as required, to align phase centers and produce the desired H(f) performance. The number of such edge elements is kept to a minimum by this design procedure. That is, for a given γ and δ specification, all other design procedures will require a larger number of τ-elements. The H(f) function characterizes elliptic filters which display Chebyshev behavior in both the pass and stopbands [2, Section 4.9] . Array substitution procedures will also be demonstrated in Section VI in a different context.

Attention is turned in the next section to a different (but perhaps more conventional) interpretation of the "stretch-and-fill" interpolation operation.

SECTION III

AUXILIARY ARRAY CONCEPT

In the interpolation discussion of Section II and Figure 2-1, the contributions of 2N stretched-seed weights toward the generation of one interpolation weight was considered in Equation (2-7). Here the process is reversed and it is noted how each particular seed weight contributes to 2N different interpolation weights. To do this Equation (2-7) is written as two separate summations, and the demand is made that the s-subscript remain constant at some fixed value, say, $\bar{k}$. For the first sum of Equation (2-7)

$$k = \bar{k} - n \tag{3-1}$$

and

$$\tau_{\bar{k}-n} = a_{-n} s_{\bar{k}}, \quad n = 1, 2, -- N. \tag{3-2}$$

For the second sum, the k value must be

$$k = \bar{k} + n - 1 \tag{3-3}$$

so that

$$\tau_{\bar{k}+n-1} = a_n s_{\bar{k}}, \quad n = 1, 2, -- N. \tag{3-4}$$

The results of Equation (3-2) and (3-4) are shown in Figure 3-1. Each seed element of Figure 2-1(b) drives an auxiliary array of 2N elements with the excitation matrix shown. Nearby seed elements similarly generate auxiliary arrays many of whose elements will coalesce with auxiliaries of other seeds. Because of superposition we may still treat these auxiliaries separately in order to demonstrate an underlying principle at work.

The pattern of the auxiliaries will first be found, then the seed element will be brought down into place (as indicated by the arrow in Figure 3-1) and the overall pattern of auxiliary with seed will be obtained. From Figure 3-1, the auxiliary array far-field pattern, $A(\theta)$, is given by (normalized to unit $s_{\bar{k}}$ current)

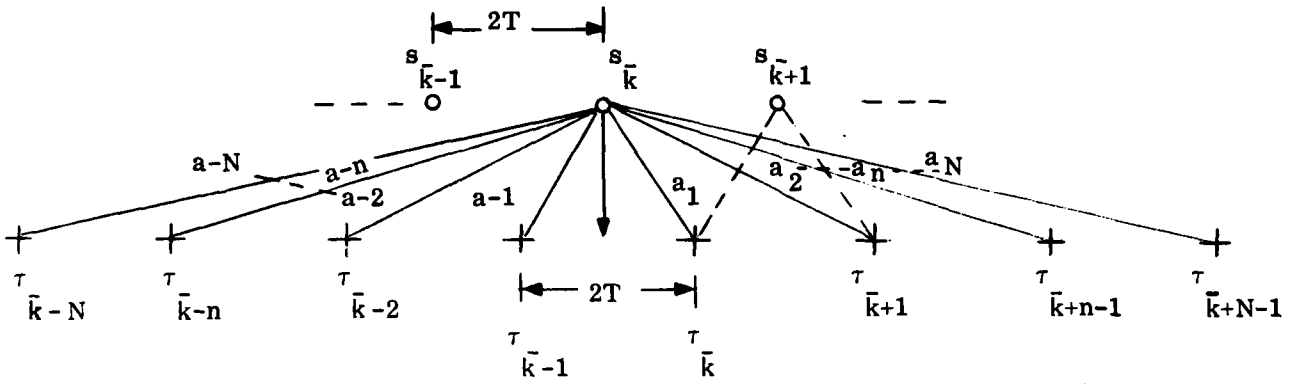

Figure 3-1. Auxiliary-Array Generated By Each Seed Element

$$A(\theta) = \sum_{n=1}^{N} a_n e^{+j2\pi (n - 1/2) \frac{2T}{\lambda} \sin\theta}$$

$$+ \sum_{n=1}^{N} a_{-n} e^{-j2\pi (n - 1/2) \frac{2T}{\lambda} \sin\theta} \quad . \tag{3-5}$$

Substitution of Equations (3-2), (3-3) and (2-14) yields

$$A(f) = \sum_{n=1}^{N} b_n \cos \pi (2n-1) \frac{f}{(R/2)} \quad . \tag{3-6}$$

Equation (1-3) may be used to show

$$A(f) = H(2f) \tag{3-7}$$

and when the $s_{\bar{k}}$ element is brought down to the center of the auxiliary array, the effective "element pattern", E(f), of the seed and its directly driven auxiliaries becomes

$$E(f) = 1 + H(2f) \ . \qquad (3\text{-}8)$$

$S_{2T}(f)$ of Figure 2-1(d) may be thought of as the array factor for the stretched seed. The factor [1+H (2f)] of Equation (3-8), which is sketched in Figure 2-1(e), becomes the "element pattern" of each seed, and its directly associated auxiliaries. The overall far-field pattern is the product of the array factor and the element pattern which becomes the $S'_T(f)$ function of Figure 2-1(f).

The auxiliary array enhances the pattern of its seed in a nearly uniform manner within the main beam. In the echelon lobe region about f = R/2 (Figure 2-1(d)). The auxiliary field cancels the seed field in a nearly uniform manner in order to produce an extended null in this region.

It has thus been demonstrated that the interpolation process of Figure 2-1 can be decomposed into a set of auxiliary arrays, one for each seed. The reinforcement in the mainlobe region and cancellation in the echelon lobe region has been explained by an element pattern anology. This viewpoint forms a useful alternate interpretation of the interpolation process. A further development of the auxiliary array concept may be found in Appendix B.

SECTION IV

PATTERN SYNTHESIS EXAMPLES

Far-field pattern specifications will be assumed to take the form of a (-3 dB) beamwidth and a peak sidelobe level. The synthesis procedure to be followed involves selection of a seed array having the requisite sidelobe suppression, but (normally) a much larger beamwidth than the specification value. An interpolation processor of the type described in Figure 1-1 (or the equivalent form of Figure 3-1) is selected having a γ value consistent with the main beam extent of the seed (as per Figure 2-1 and associated discussion). The stopband suppression level of the interpolator is chosen to meet the peak sidelobe specification for the final array, and is usually a match to the seed-sidelobe level. The array element spacings are assumed held throughout to some prespecified value.

The desired far-field pattern is achieved by scaling the seed pattern repeatedly through interpolation stages until the specified beamwidth is achieved. The required scaling factor F_r is given by

$$F_r = \frac{\sin B_{s/2}}{\sin B_{r/2}} \tag{4-1}$$

where B_s is the seed -3 dB beamwidth and B_r is the required (specification) -3 dB beamwidth. If F_r is a power of 2, then $\log_2 (F_r)$ will yield the number of levels of interpolation that will be required. If such is not the case one may use a number of interpolation levels in excess of the $\log_2 (F_r)$ value and then one may resample the resulting array (select every J^{th} element) such that

$$F_r \cong \frac{2}{J}^{L} \tag{4-2}$$

where L is the number of interpolation levels used [1, Section 5.4] . An example of such a "J-derived" array will be shown later.

An alternate solution to this problem involves variation of seed design so that the resulting value of B_s in Equation (4-1) will yield a power of two for F_r. The quantization forced on the designer (e.g. number of seed elements, number of interpolator coefficient pairs) can be annoying, but such is the nature of the problem. By maintaining a discrete design approach throughout, one avoids surprises that sometimes occur in continuous/discrete conversions. This is especially helpful when the final array contains a small number of elements.

The synthesis examples to be given here do not necessarily represent optimum designs. Readily available procedures were selected for convenience. For example, the interpolation processor used in these examples was originally designed for other purposes [1, Section 4.2] . As shown in Table 4-1 four interpolator designs were used having nominal suppression levels of -25, -40, -50, and -65 dB, all at a γ value of 0.8. The Chebyshev seeds were then designed for a matching mainlobe region (sidelobe level reached at $f = \gamma R/2$) and sidelobe levels as close to the interpolator values as could be obtained. As seen from the table, the sidelobe match is not really very good except for the -25 dB case. It might also be mentioned that the interpolators use an "extended gamma" design at second level [1, Section 3.2] which is really not necessary for this application. Hence the interpolators are actually somewhat overdesigned for the intended purpose.

Some examples for a -25 dB nominal sidelobe level are shown first. The three-element seed pattern which is used for this set is shown in Figure 4-1. In all of these plots a normalized $\sin\theta$ variable, $x=\sin\theta/(R/2)$, is the abscissa variable. The sidelobe region starts at x=0.8, and has a null at x=0.86. The sidelobe response rises to the specified peak value at x=1. The x=1 value is a "foldover" value for the pattern; that is, the patterns are symmetric about x=1. Thus if Figure 4-1 were continued to x=2, there would be a null at x=1.14 and the mainlobe region centered at x=2 would begin x=1.2. If the seed array spacing were doubled, all these x-values would, of course, be halved.

The pattern resulting from a single interplation level is shown in Figure 4-2. This figure will be examined so as to identify first the effects of stretching and then the effects of interpolation. If stretching only were involved, the original sidelobe region ($0.8 \leq x \leq 1$) would now appear from ($0.4 \leq x \leq 0.5$) with the original sidelobe null at 0.86 appearing at 0.43. These effects are clearly indicated in Figure 4-2. The sidelobe continuation in x would now fall at ($0.5 \leq x \leq 0.6$) with a null at x=0.57. The pattern would then build from x=0.6 to a second mainlobe peak at (0-dB level) at x=1.

The effects of the interpolator may now be understood relative to Figure 4-2. A flat response is maintained from 0 to 0.4. A transition region (see Figure 2-1(e)) extends from 0.4 to 0.6 and the "stopband" region extends from 0.6 to 1.

The nulls in the pattern beyond x=0.6 are due to the interpolator as is the pattern level at x=1. (Without the interpolator the level at x=1 would be 0 dB). In the transition region the interpolator contributes 0-dB loss at x=0.4, -6dB loss at x=0.5, and its design stopband loss (about -26 dB in this case) in the region ($0.6 \leq x \leq 1$). This behavior can be verified by close examination of Figures 4-1 and 4-2.

TABLE 4-1

PARAMETERS USED IN EXAMPLES

Figure No.	No. of Seed Elements	Inter-polator Type	Inter-polation Level	No. of Elements	Element Count After Truncation	Beam-width (1)	Side-lobe Spec	Apper Effic η	Comments
4-2	3	4	1	15	-	17.38	-25	0.403	
4-3	3	4	2	35	-	8.91	-25	0.339	
4-4	3	4	3	71	-	4.42	-25	0.336	
4-6	4	3	1	25	-	16.45	-40	0.270	
4-7	4	3	2	59	-	8.15	-40	0.230	
4-8	4	3	3	123	-	4.09	-40	0.221	
4-9	1	3	1	19	-	55.84	-40	0.114	Omnidir. Seed
4-10	1	3	3	99	-	13.46	-40	0.088	Omnidir. Seed
4-11	5	2	3	171	-	3.67	-50	0.177	
4-12	6	1	3	239	-	3.27	-65	0.140	
5-3	3	4	2	35	13	10.03	-25	0.847	Truncation of Fig 4-3 Array
5-4	3	4	9	4607	13	12.25	-25	0.692	J-Derived Array, See Text
5-6	4	3	3	123	47	4.14	-40	0.567	Truncation of Fig 4-8
5-8	5	2	3	171	55	3.64	-50	0.547	Truncation of Fig 4-11
5-9	5	2	4	347	56	3.67	-50	0.537	Even Element Case, See Text
5-11	6	1	3	239	71	3.27	-65	0.471	Truncation of Fig 4-12

a) Far-Field Pattern Plot Details

TABLE 4-1 (CONT)

PARAMETERS USED IN EXAMPLES

NT	γ	δ (dB)	Design Type
1	0.8	-65	Extended γ
2	0.8	-50	Extended γ
3	0.8	-40	Extended γ
4	0.8	-25	Extended γ
10	0.6	-50	Normal

b) Interpolator Data

Figure No.	No. of Elements	Beamwidth (1)	Sidelobe Level (dB)
4-1	3	38.44	-26.43
4-5	4	33.52	-42.07
-	5	29.35	-58.00
-	6	26.34	-73.99

c) Seed Pattern Data

Notes:

1) -3 dB values in degrees based on half wavelength element spacing.

2) Aperture efficiency = η

No. of elements = K

Complex element weights = $\hat{W}_k$

$$\eta = \frac{\left| \sum_{k=1}^{K} \hat{W}_k \right|^2}{K \sum_{k=1}^{K} \left| \hat{W}_k \right|^2}$$

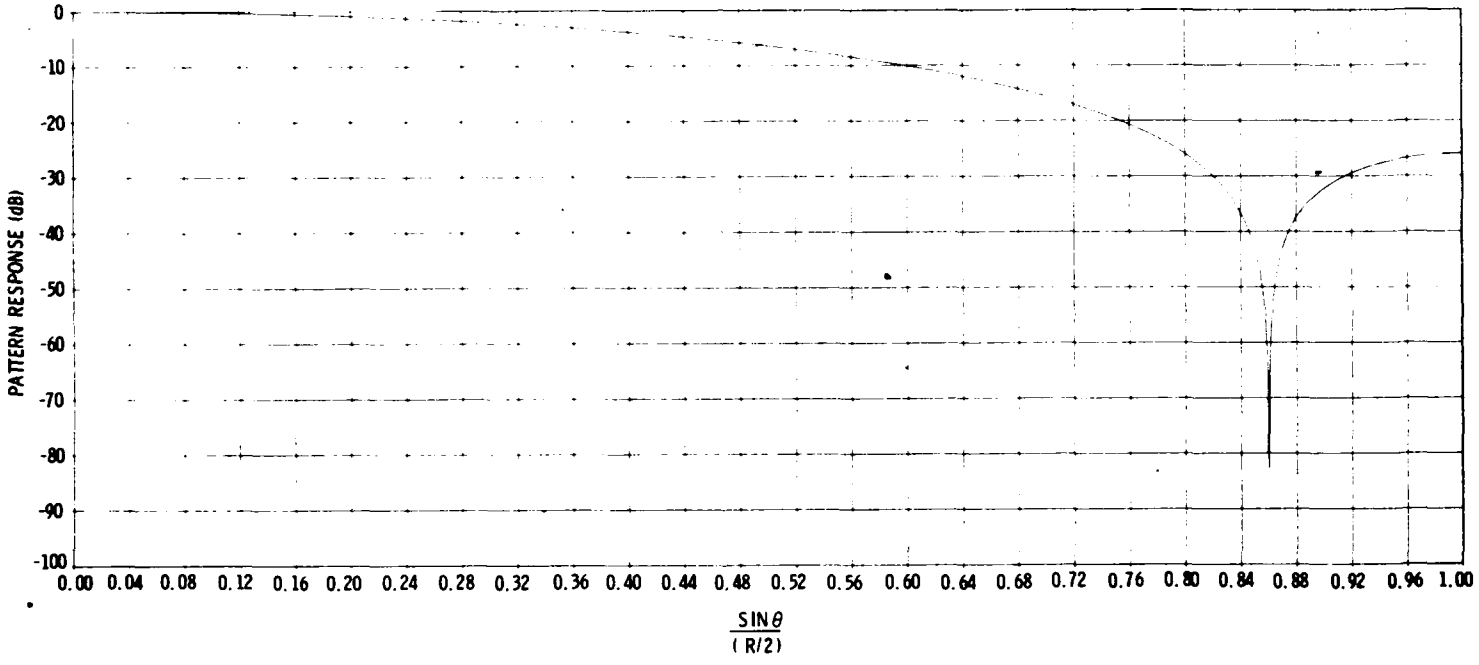

Figure 4-1. Three-Element Seed Pattern Used For -25 dB Design

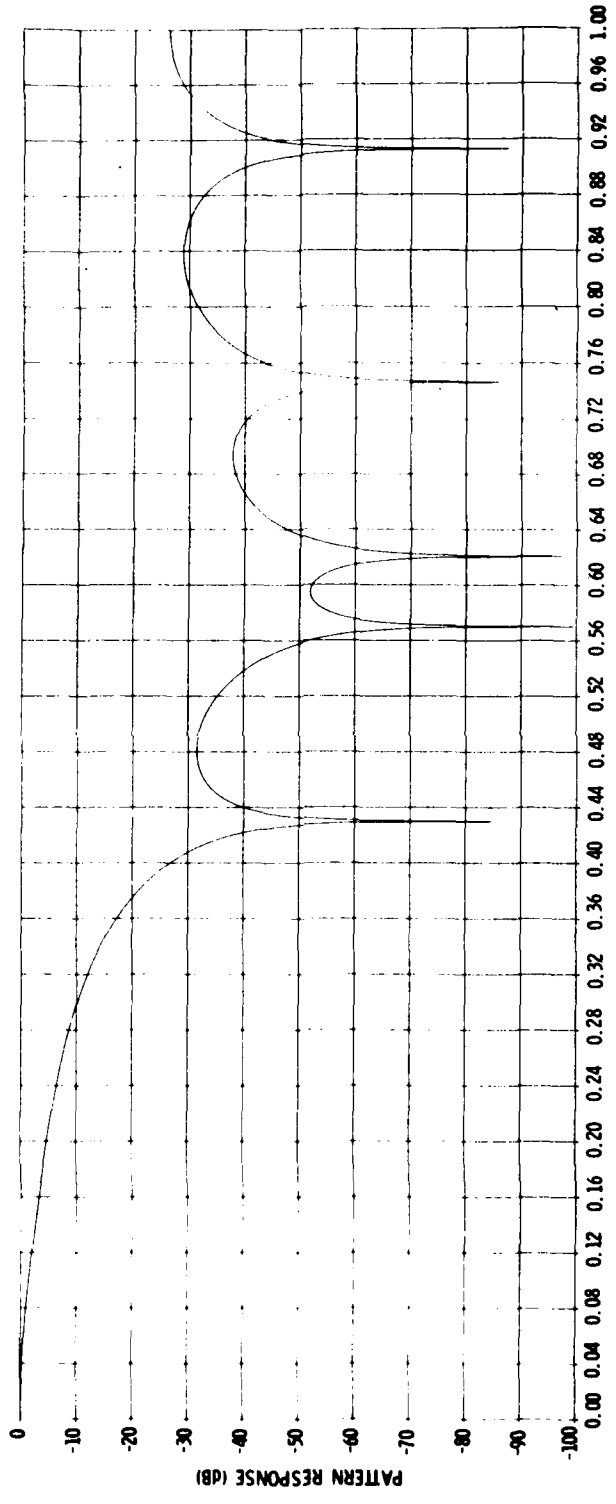

Figure 4-2. Pattern of 3-Element Seed After 1-Interpolation Level (-25 dB Design)

The pattern after a second interpolation level is shown in Figure 4-3, and after three interpolation levels is demonstrated in Figure 4-4. This process may be continued indefinitely to arrive at any desired final beamwidth, no matter how small this may be.

It will be noted in Figure 4-3 and 4-4 that the peak sidelobe levels have dropped noticeably below the -25 dB specification value. This is a routine occurrence for the higher interpolation cases and is caused by two main factors. First, the behavior of each interpolator in the transition region adds some additional attenuation to "specification level" sidelobes squeezed into that region by the stretching process. Secondly, the design of the interpolators becomes simpler at the higher interpolation levels since the effective value of γ is reduced by a factor of one-half at each level. This generally means that an interpolator having a smaller number of coefficient pairs (N value of Equation (2-7)) may be selected. At the smaller N values quantization becomes a factor. An interpolator at some level using N = K does not quite provide enough stopband attenuation while the N = K+1 design provides an excess of echelon lobe suppression. One always opts, of course, for the K+1 choice in designing the interpolator chain.

The use of an overdesigned interpolator chain produces lower than specified sidelobe levels at the expense (mainly) of the creation of a larger than necessary number of "end-effect" elements at the array edges. Many of these elements have such small excitation levels that they may be removed without doing serious harm to the pattern. When truncation is properly done, the sidelobe peak response may be maintained at specification level while the aperture size is reduced to values consistent with the achieved beamwidth and sidelobe level. For this reason the element counts for the arrays of this section should not be given much significance. This topic is dicussed in more detail in Section V.

Figure 4-5 shows the four-element Chebyshev pattern used as the seed for the next set of examples having a nominal -40 dB sidelobe specification. This seed yields peak sidelobe levels of -42 dB while the interpolator has a -38 dB stopband, so that a quantization-forced mismatch exists. Figure 4-6 shows the pattern after one level of interpolation. The points of interest here may be examined by using the general arguments relative to Figures 4-1 and 4-2 on Figures 4-5 and 4-6. The more complex nature of the interpolator of Figure 4-6 is indicated by the number of nulls between x=0.6 and x=1 as compared to the same region of Figure 4-2. (This is the echelon lobe region in both cases.)

The pattern after two and three interpolation levels is shown in Figures 4-7 and 4-8 respectively. These last two figures show regions of very-deep sidelobe levels in addition to a peak level that tends to fall below the nominal -40 dB design value.

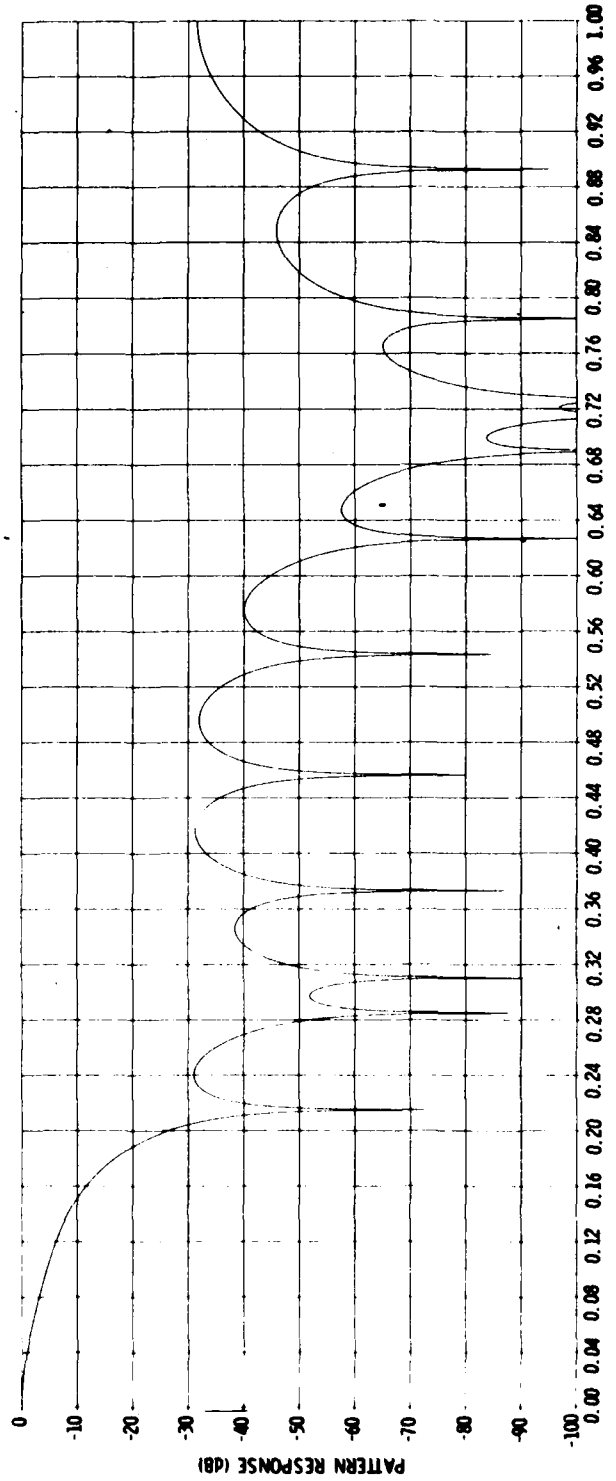

Figure 4-3. Pattern of 3-Element Seed After 2-Interpolation Levels (-25 dB Design)

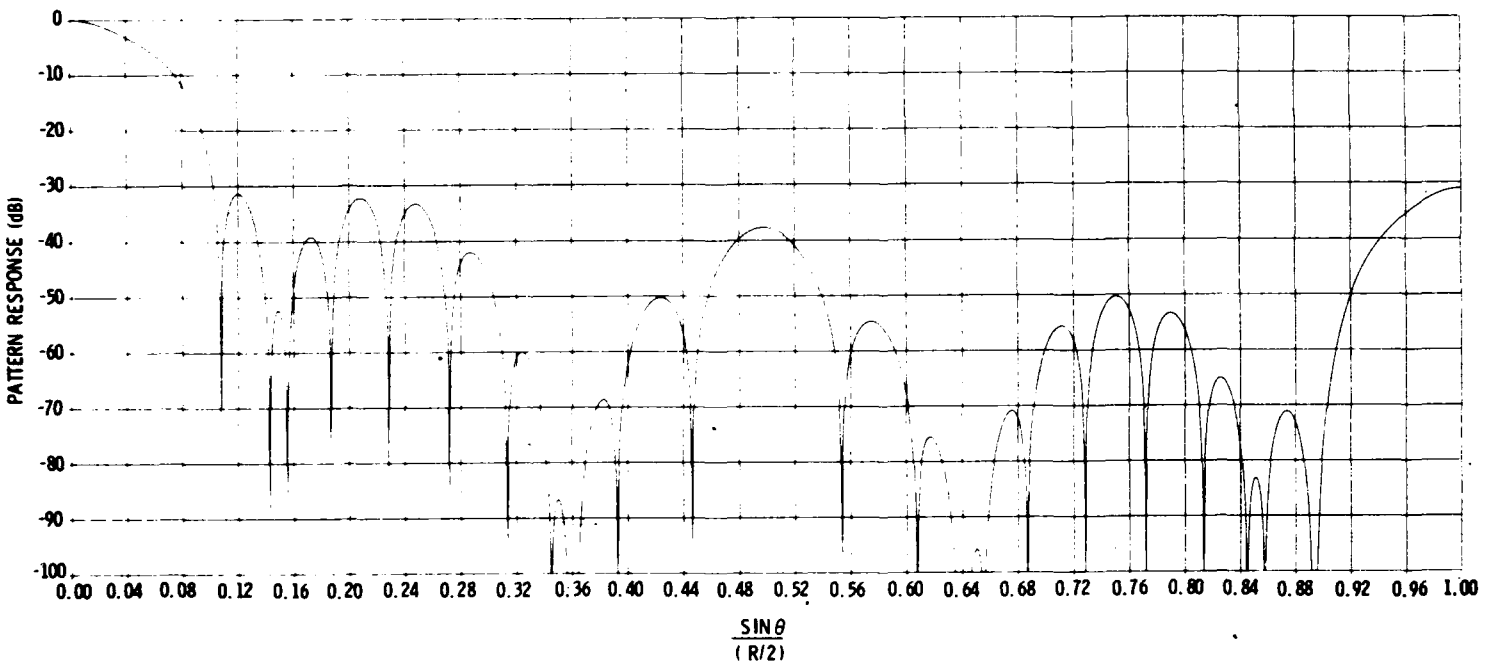

Figure 4-4. Pattern of 3-Element Seed After 3-Interpolation Levels (-25 dB Design)

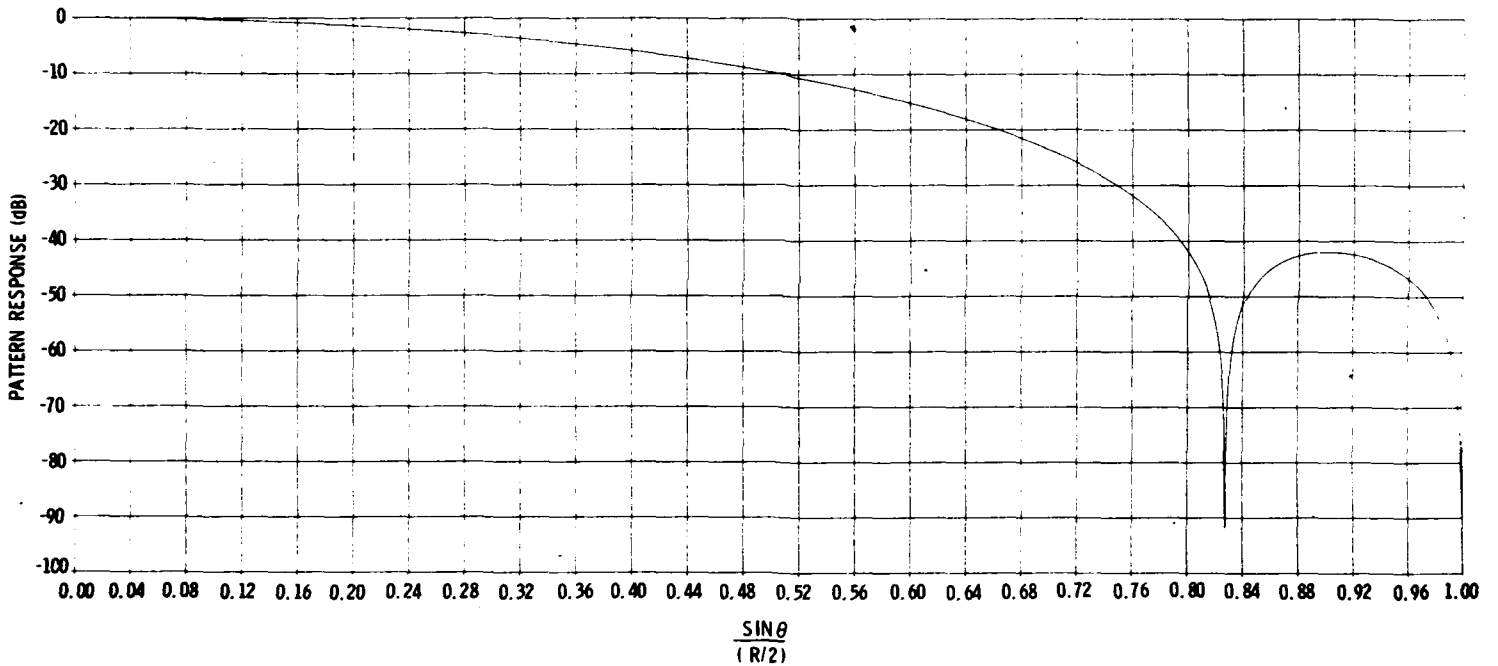

Figure 4-5. Four-Element Seed Pattern Used For -40 dB Design

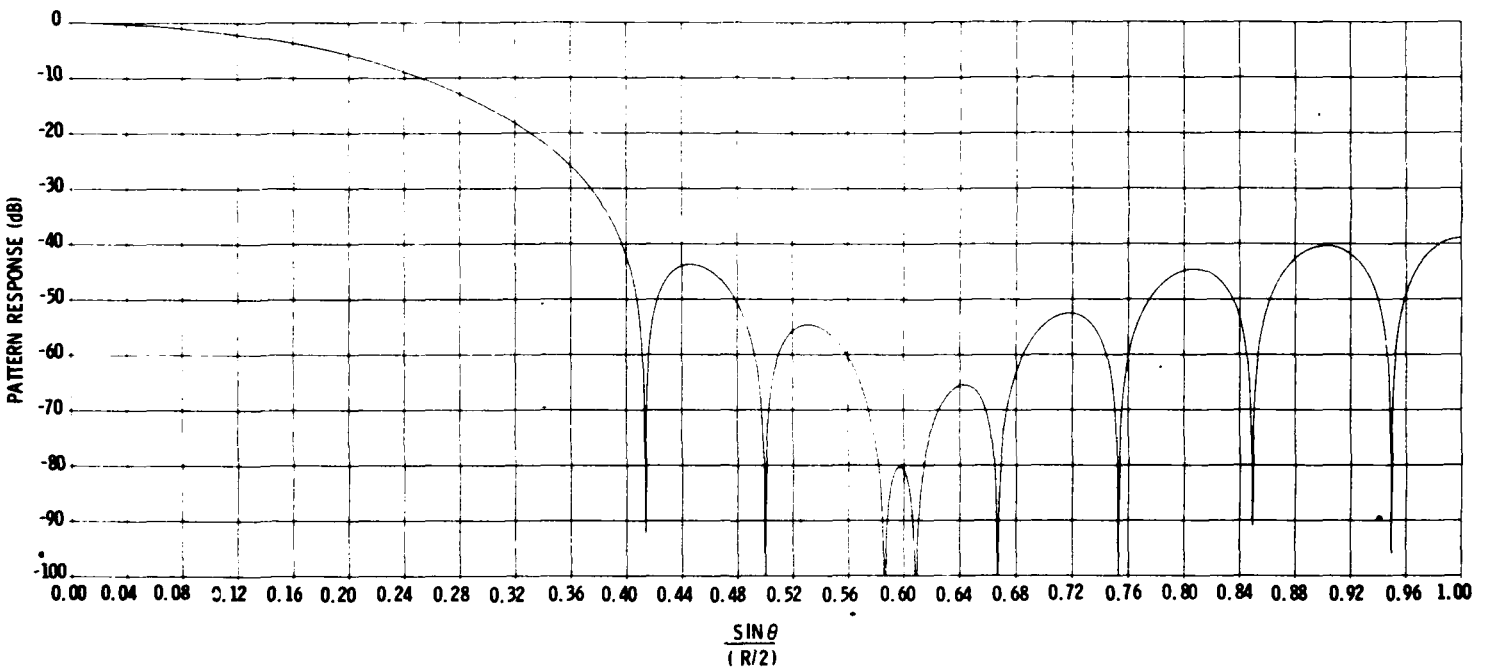

Figure 4-6. Pattern of 4-Element Seed After 1-Interpolation Level (-40dB Design)

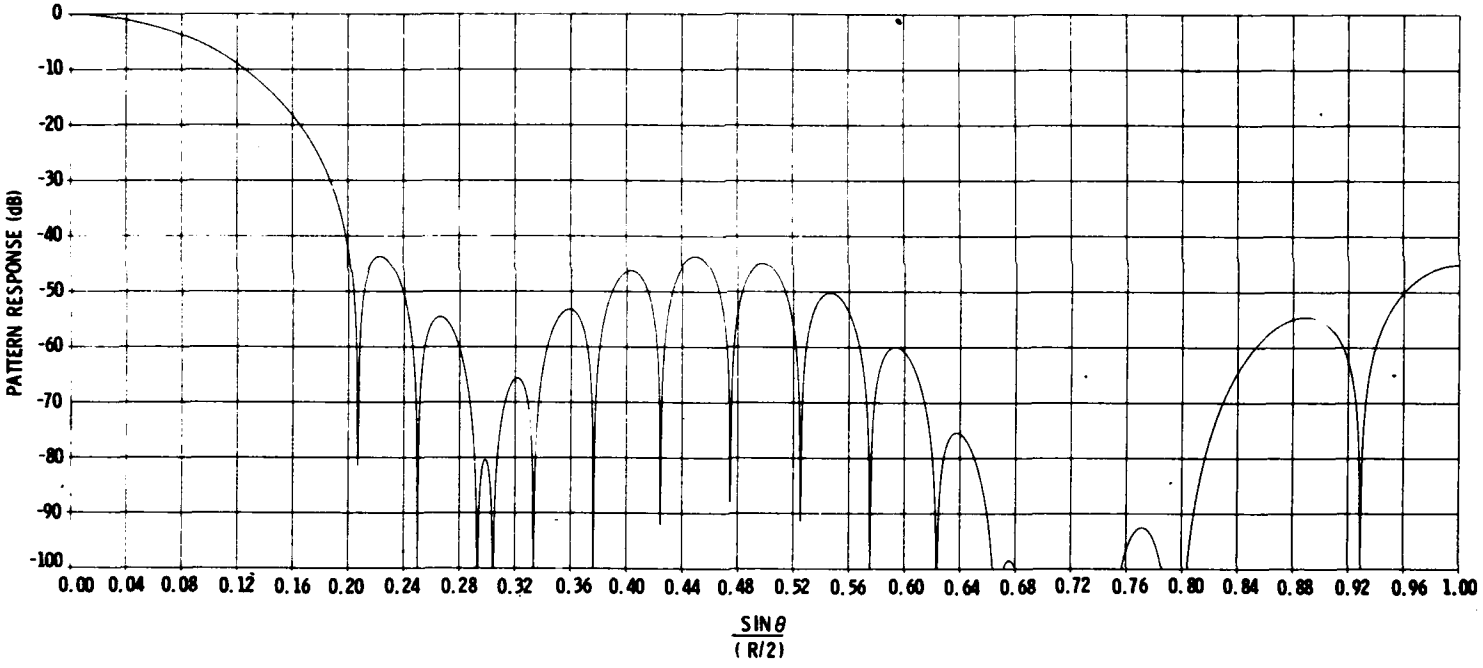

Figure 4-7. Pattern of 4-Element Seed After 2-Interpolation Levels (-40 dB Design)

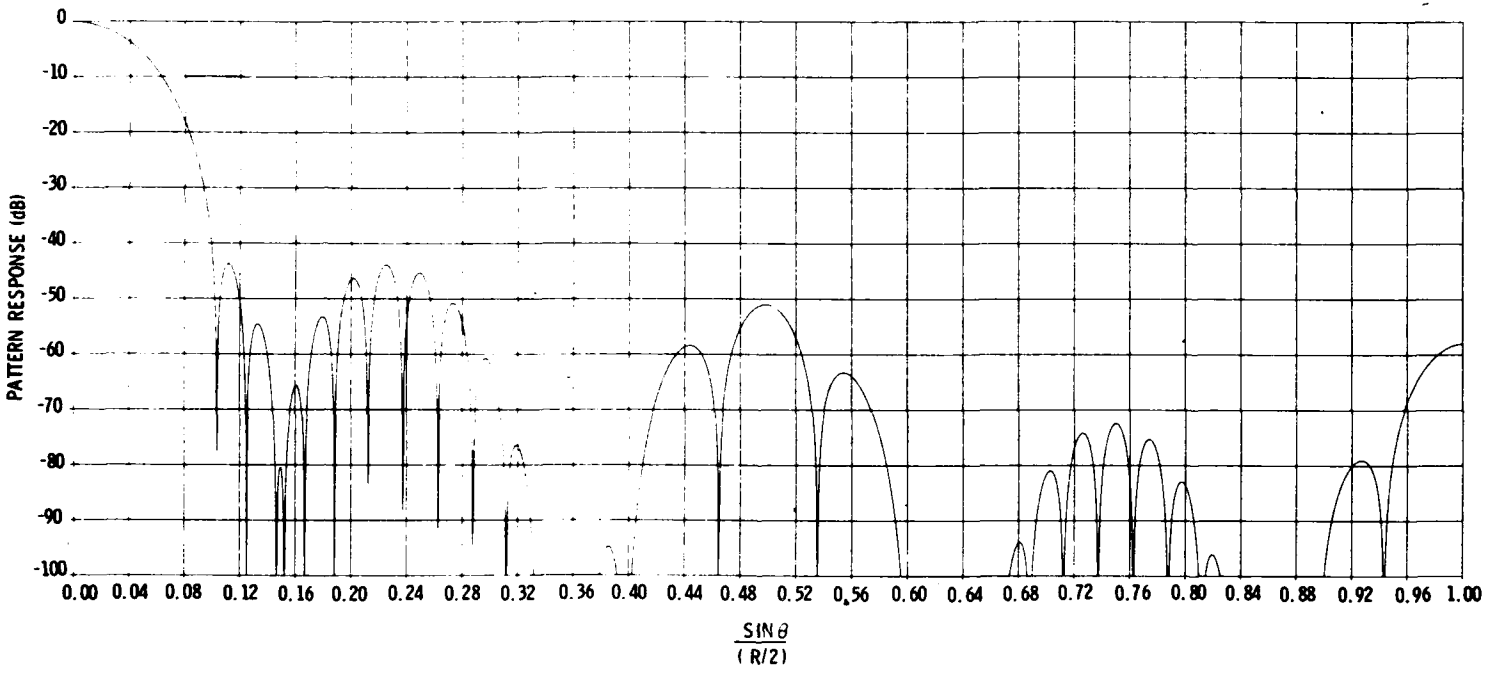

Figure 4-8. Pattern of 4-Element Seed After 3-Interpolation Levels (-40 dB Design)

The pattern which results when a single-element (omnidirectional) seed is used is shown in Figure 4-9. The seed provides a "mainlobe" region at all angles, hence the pattern at first level reveals the workings of the interpolator. In Figure 4-9 a uniform response is maintained from x=0 to x=0.4. The transition region extends from 0.4 to 0.6, while the stopband region extends from x=0.6 to x=1. The null pattern beyond x=0.6 of Figure 4-9 may be compared to the same region of Figure 4-6. The stopband behavior of the interpolator in the echelon lobe region of Figure 4-6 is identified quite easily.

The omnidirectional seed pattern after two levels of interpolation is shown in Figure 4-10. The "mainlobe" region is scaled down by a factor of two as compared to Figure 4-9. While these last two figures are presented as oddities, there may be practical cases in which a uniform response in the main beam is desired accompanied by a rapid transition to the sidelobe region. Such patterns can be obtained by the methods outlined here. Additional comments on this subject will be made in Section V.

For a nominal -50 dB design a five-element seed is used. After three levels of interpolation, the resulting pattern is shown in Figure 4-11. The nominal -65 dB design uses a six-element seed whose pattern after three interpolation levels is shown in Figure 4-12. In both cases the drop in peak sidelobe level below the nominal peak value is to be noted. The extended areas of very low sidelobe level are also to be noted in these two figures. These last two cases are presented mainly to illustrate some points to be detailed in Section V.

Table 4-1 summarizes some of the data items involved in the pattern figures shown here and in Section V.

Extensions of the technique to greater sidelobe suppression and/or narrower beamwidth are routine. The few cases shown here are meant only to illustrate design principles which will be further defined in the next section.

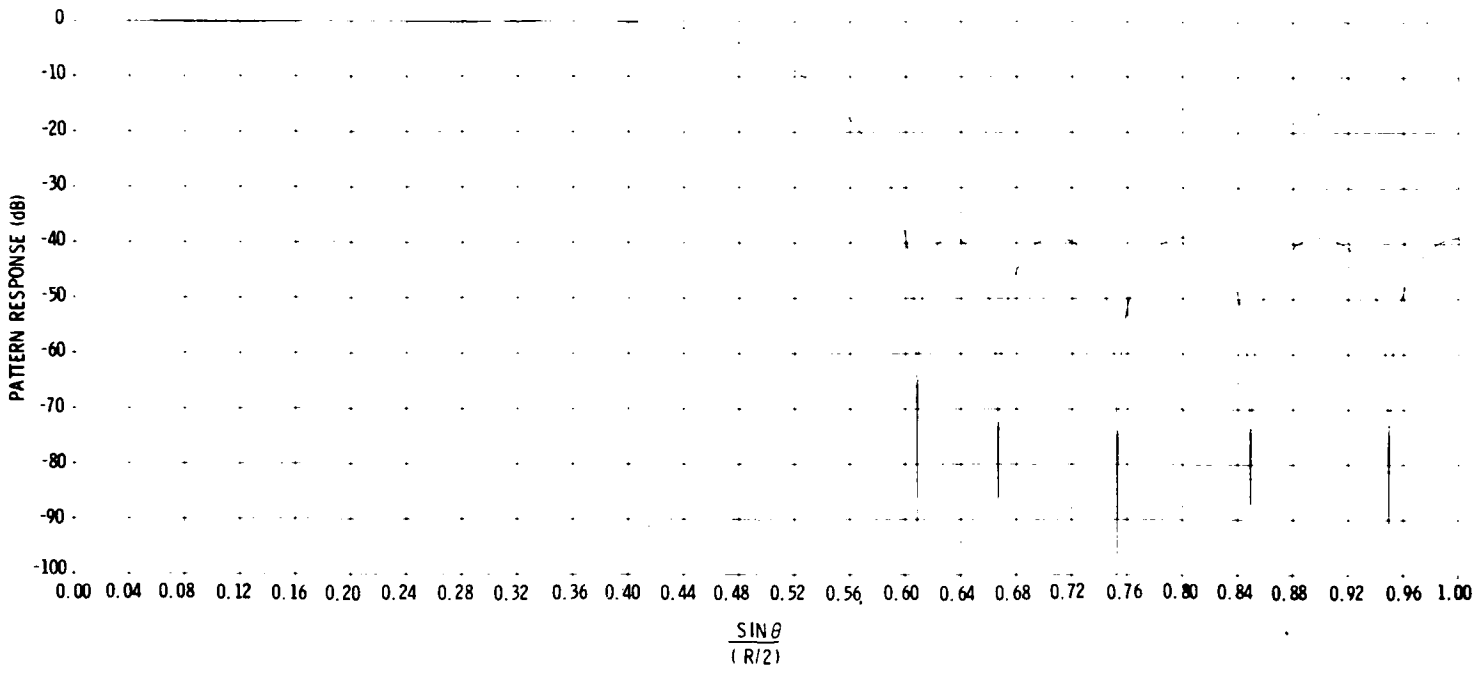

Figure 4-9. Pattern of Single-Element (Omni) Seed After 1-Interpolation Level (-40 dB Design)

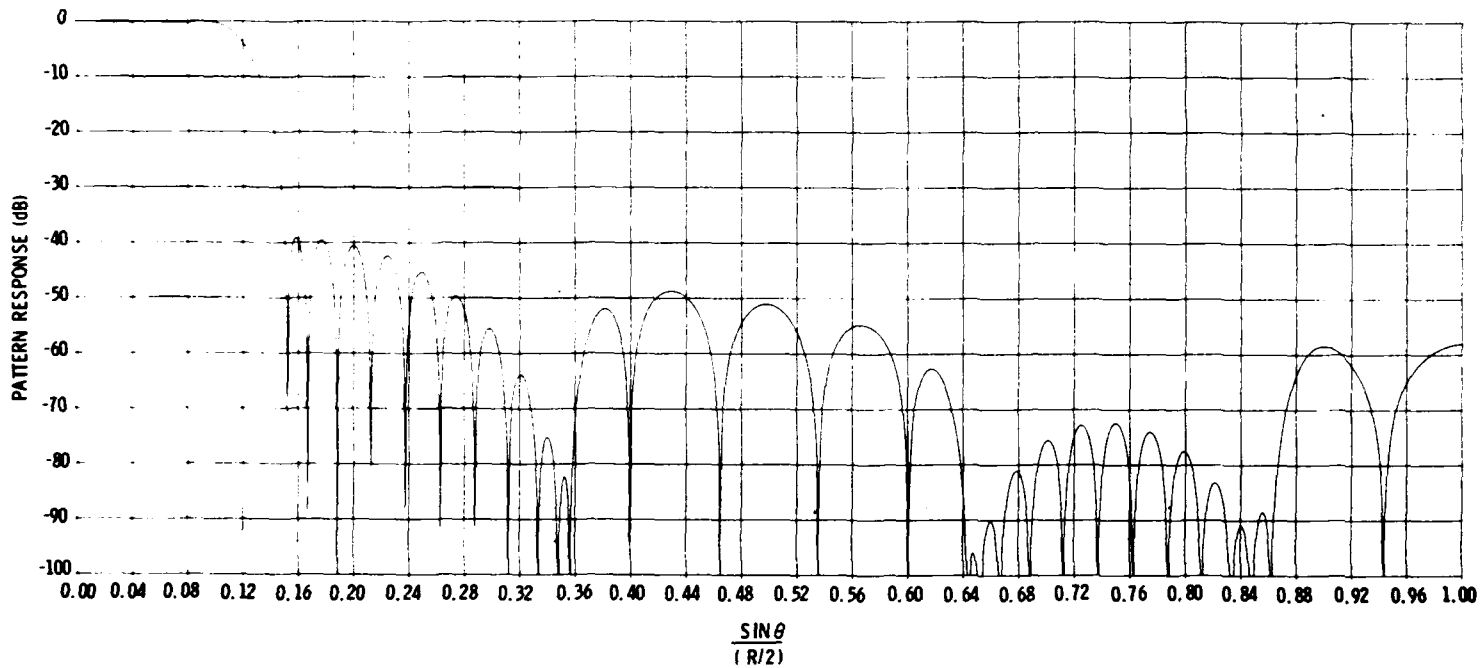

Figure 4-10. Pattern of Single Element (Omni) Seed After 2-Interpolation Levels (-40 dB Design)

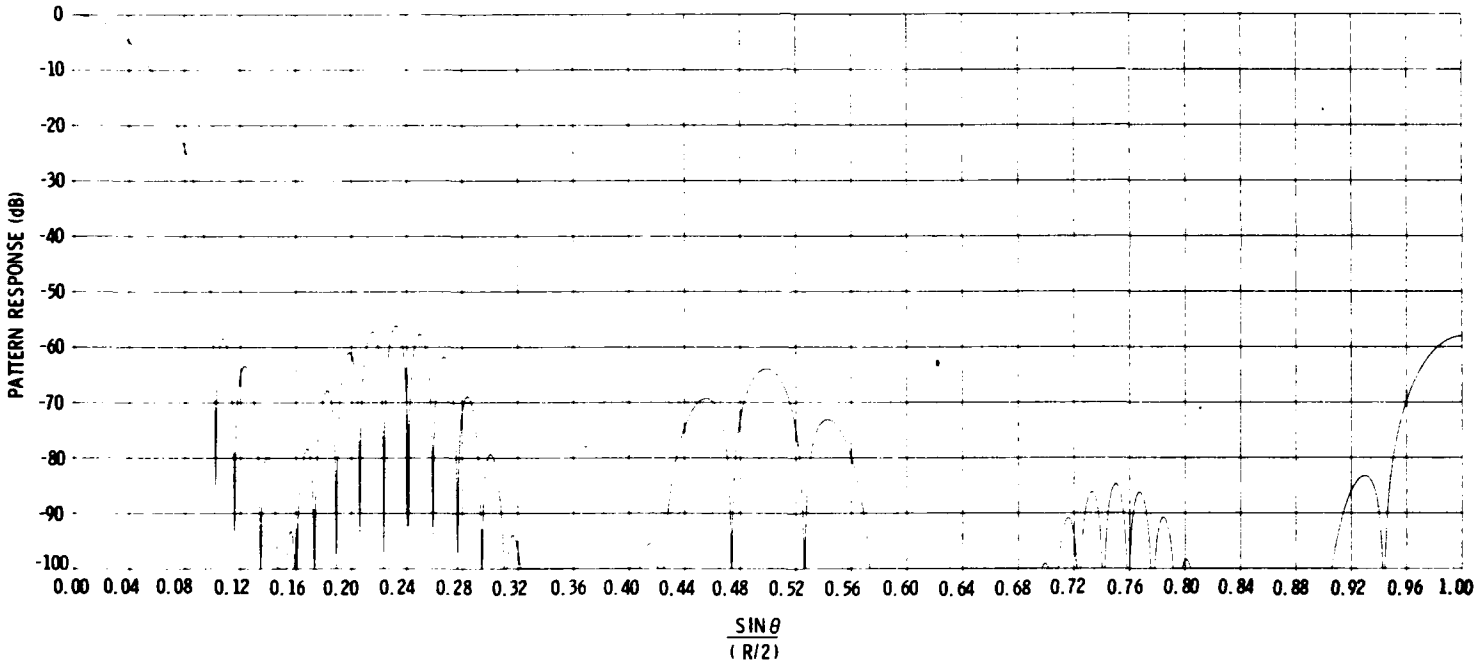

Figure 4-11. Pattern of 5-Element Seed After 3-Interpolation Levels (-50 dB Design)

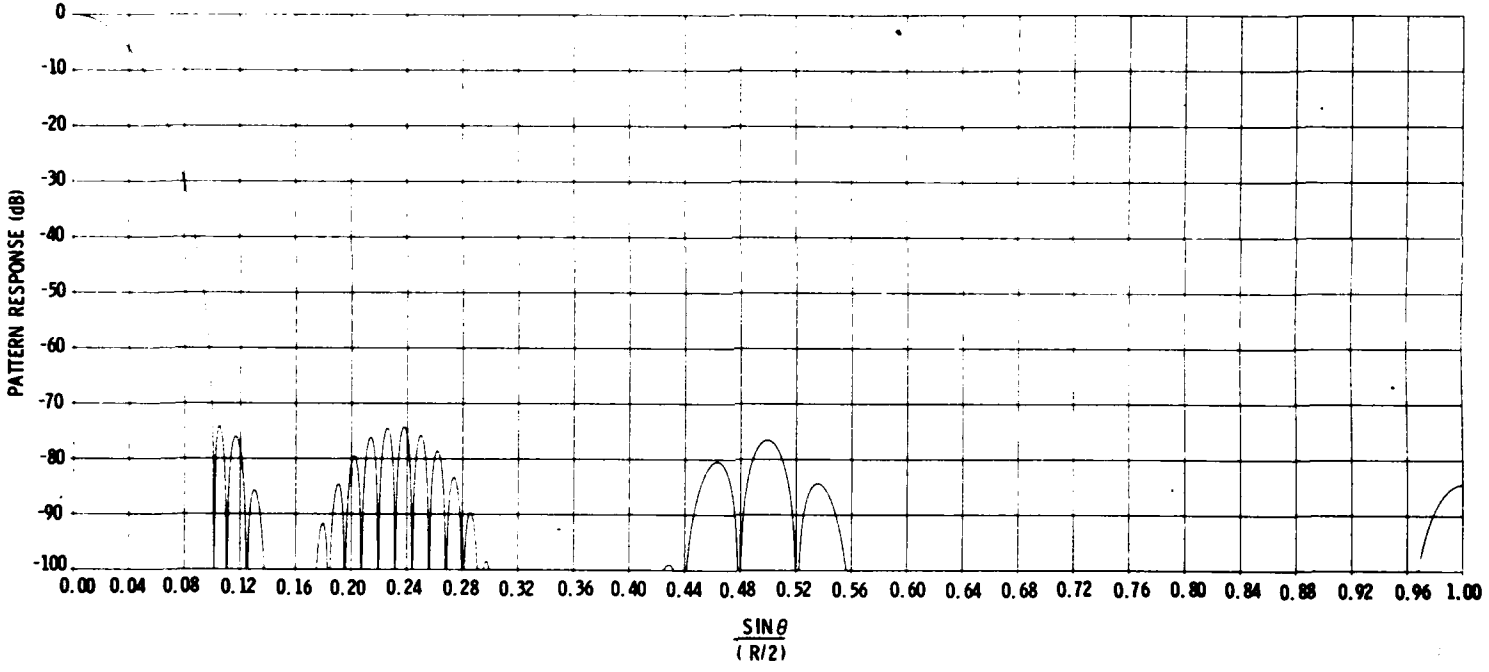

Figure 4-12. Pattern of 6-Element Seed After 3-Interpolation Levels (-65 dB Design)

SECTION V

CURRENT DISTRIBUTIONS AND END-EFFECT TRUNCATION

In previous work the interpolation processor has been used to create array element weights and attention has been focused on the far-field patterns resulting from these weights. In this section attention will be turned to the nature of array excitation.

In the context of Figure 2-1 and Equation (2-7), an equivalent interpolator structure may be configured as shown in Figure 5-1. This arrangement avoids the "reverse-order" entry of seed values as required by the Figure 1-1 arrangement. It is convenient to think of the processor of Figure 5-1 as being moved under the stretched-seed array producing, at each stop, an interpolation value. If this process is done repeatedly on a multilevel basis, it may be shown that the number of coefficients (elements) at level L is

$$C_L = (C_0 - 1)\, 2^L + 2 \sum_{k=1}^{L} 2^{(L+1-k)} N_k - 2^{L+1} + 3 \qquad (5\text{-}1)$$

where C_0 is the number of elements at zero level (the number of seed elements), and N_k is the number of coefficient pairs at level k in the interpolator used.

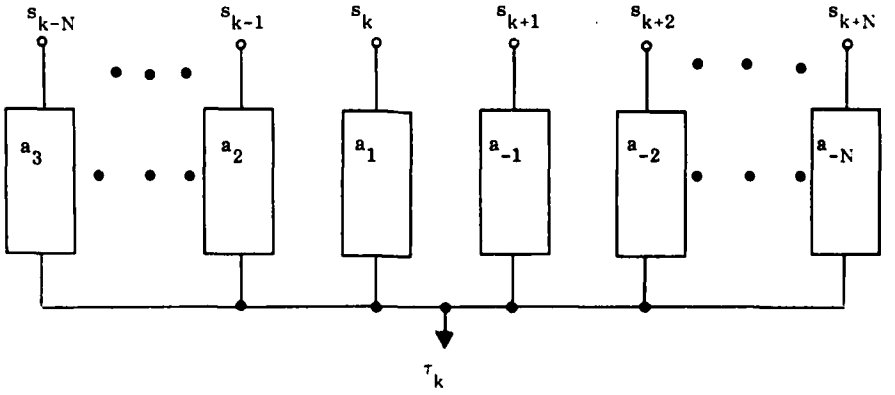

Figure 5-1. Interpolation Processor Realization

Since every weight at every level appears in the final array, the original seeds appear in the final array. We define as "internal" elements of the final array, the seeds and all elements between seed elements. By "external" elements those end elements are meant which are found outboard of the outermost seed elements. The number, C_I, of interior elements is

$$C_I = (C_0-1)\, 2^L + 1 \tag{5-2}$$

and the number, C_E, of exterior elements at each end of the array is

$$C_E = \sum_{k=1}^{L} 2^{(L+1-k)} N_k - (2^L - 1) \tag{5-3}$$

so that

$$C_L = C_I + 2 \times C_E \tag{5-4}$$

In typical first-cut designs such as those discussed in Section V, the exterior elements comprise 75 to 80 percent of the array. The excitation levels in these elements decrease rapidly with distance from array center and a high percentage of these elements may be discarded in an aperture truncation operation without invalidating the far-field pattern specifications.

The nature of this aperture illumination , is easily explained using Figure 5-1. The first interpolator coefficient will be generated at level one when the a_{-N} weight falls under the first seed element. A small value results since only one seed contributes; also, the end weights of the interpolator coefficient set tend to be small. (Note too that alternate weights in this region are zero since there is nc seed "brought-down" between interpolation values.) Thus, processor "build-up" and "build-down" regions are found at each end of the level one array. This process is repeated at all levels except that beyond level one previous "build-up" regions interact first with the processor at that level, and the tendency to create many low-level elements at the array ends is exacerbated.

This characteristic of the procedure is also heightened by use of overly complex interpolation processors as may be forced on the designer by the tyranny of quantization in the choice of N as discussed in the previous section. An important advantage of this procedure, however, is the smooth decay of the illumination function that always results.

As will be seen, the weight function is not quite monotonic, but is nearly so in the examples to be reviewed.

By nature of this process, the weight distribution for a given level value contains the excitation information for all levels less than the one shown. (Selection of the center element and every other element at level L yields the level L-1 array, etc.) For this reason aperture functions for L=5 will be shown even though far-field patterns for lesser L-values are of direct concern.

Figure 5-2 shows the level 5 weight distribution for the -25 dB design. In these figures bar graphs would be truly representative of discrete-array illumination. However, the point-to-point plots presented will serve since the point density is high. In Figure 5-2 there are over 14 element values per major division. Selecting the center and then every 16^{th} element of this array yields the pattern of Figure 4-2, every 8^{th} element gives the Figure 4-3 and selection of every 4^{th} element produces the far-field pattern of Figure 4-4.

The level two pattern of Figure 4-3 is generated by an array of 35 elements taken from the weight distribution of Figure 5-2. By symmetrically truncating this 35-element array so as to discard low-weight edge elements, a 13-element array having the pattern shown in Figure 5-3 results. Truncation is very easily done using an interactive computer program which allows pattern effects to be observed as elements are discarded. One merely stops the process when further truncation would violate a specification.

In this high-sidelobe example truncation does slightly modify main beam shape but the main effect is in the sidelobes. Comparing Figures 5-2 and 4-3 shows that the main contribution of the outboard, low-level elements is extra sidelobe suppression as argued in the previous section. Truncation removed 22 of 35 elements or 63% of the reference array. The span of elements kept after truncation is indicated by the T-region of the weight plots. (In all of the weight plots shown here the outermost seeds will fall at about 0.4 and 0.6.)

The opportunity to obtain mainlobe scaling factors which are other than a power of two, was outlined previously, and is demonstrated in Figure 5-4. A level 9 scaling was used (512:1) which was later resampled by a J-step of 163 to obtain an effective scaling of $512/163 = 3.14$ for demonstration purposes. This was in turn truncated to 13 elements yielding the far-field pattern shown in Figure 5-4.

Figure 5-5 shows the aperture illumination for the -40 dB design. There are about 25 elements per division in this plot. At this lower sidelobe level a relatively smooth current distribution results. Using every 4^{th} element from this aperture gives the 123-element reference array of Figure 4-8. When this is truncated to 47 elements the pattern

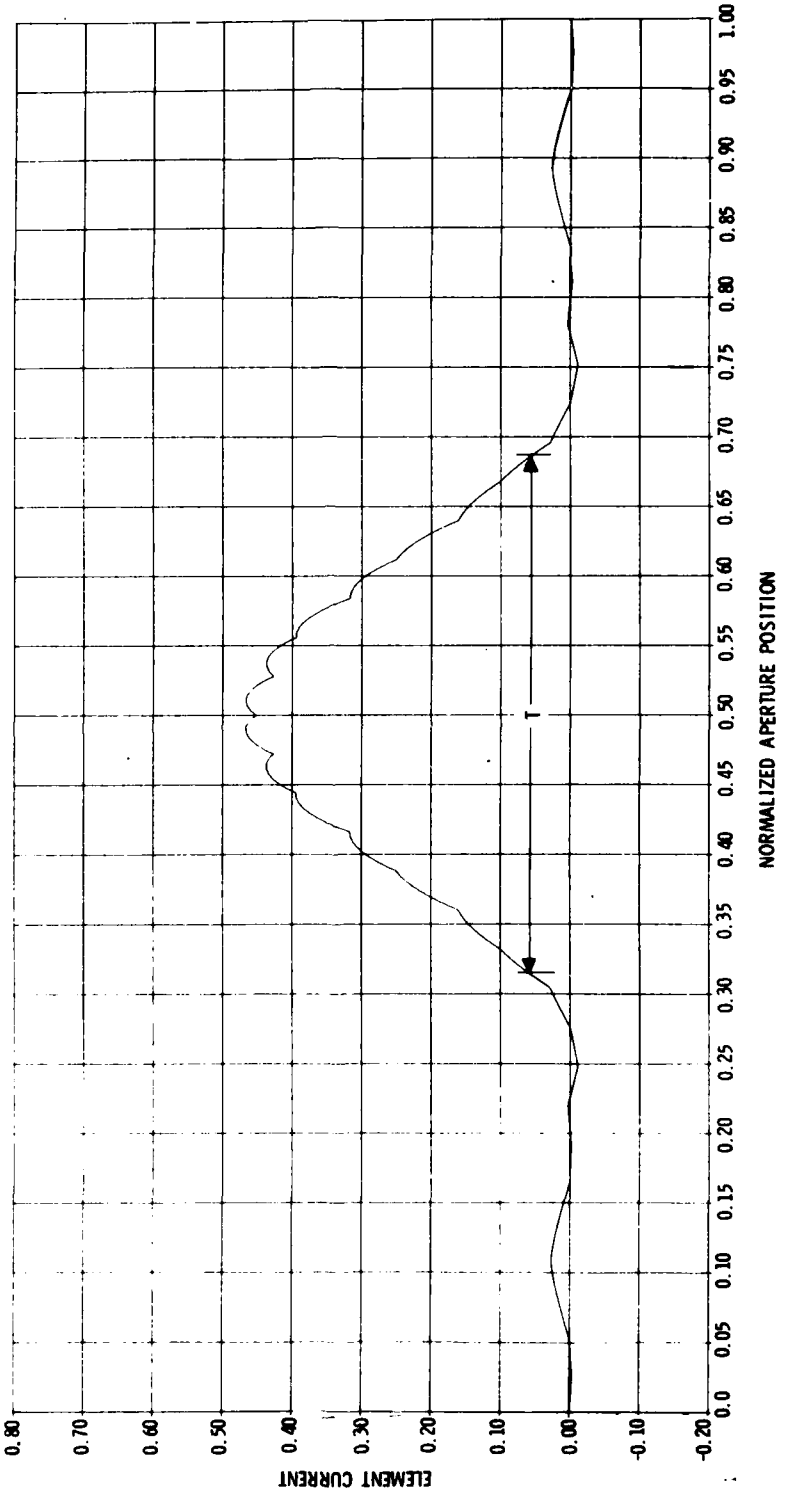

Figure 5-2. Current Distribution, -25 dB Design, 287 Points, L=5 (End Seeds at 0.39 and 0.61)

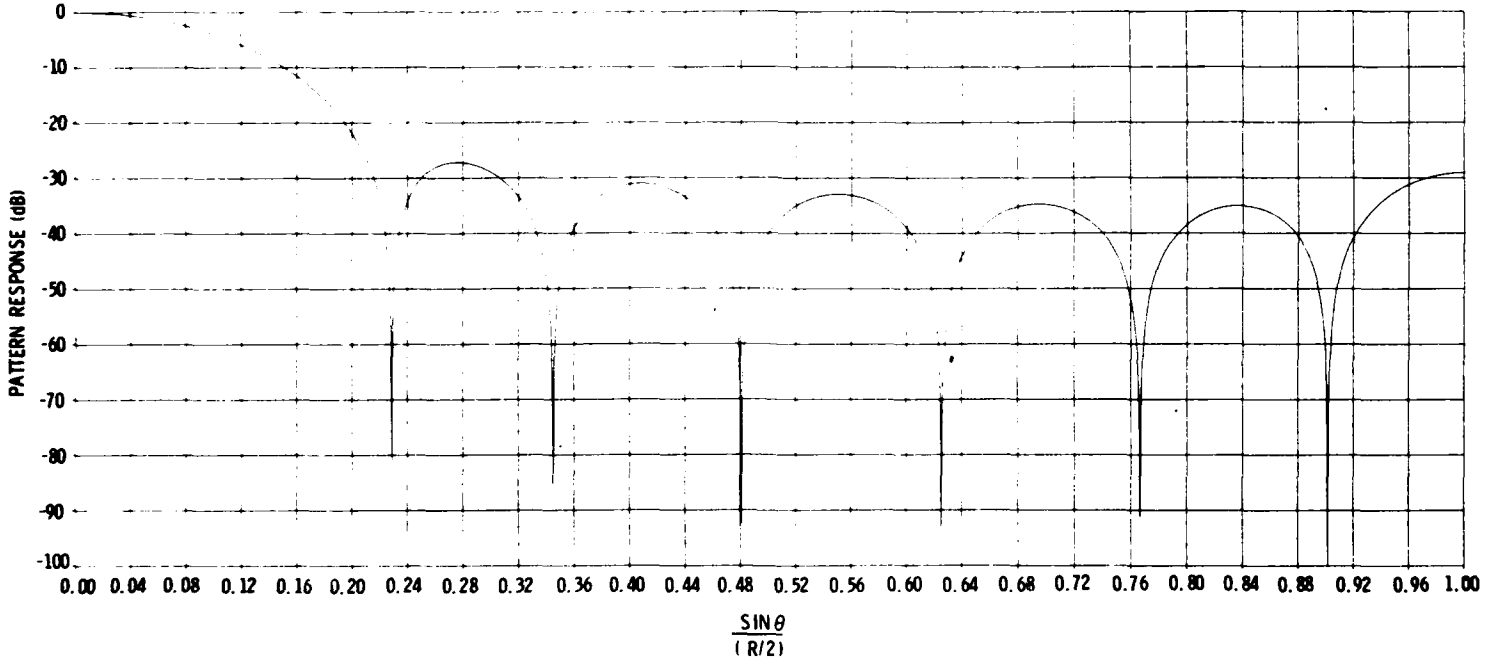

Figure 5-3. Pattern of -25 dB Design Level 2 Array Truncated to 13 Elements from an Original 35

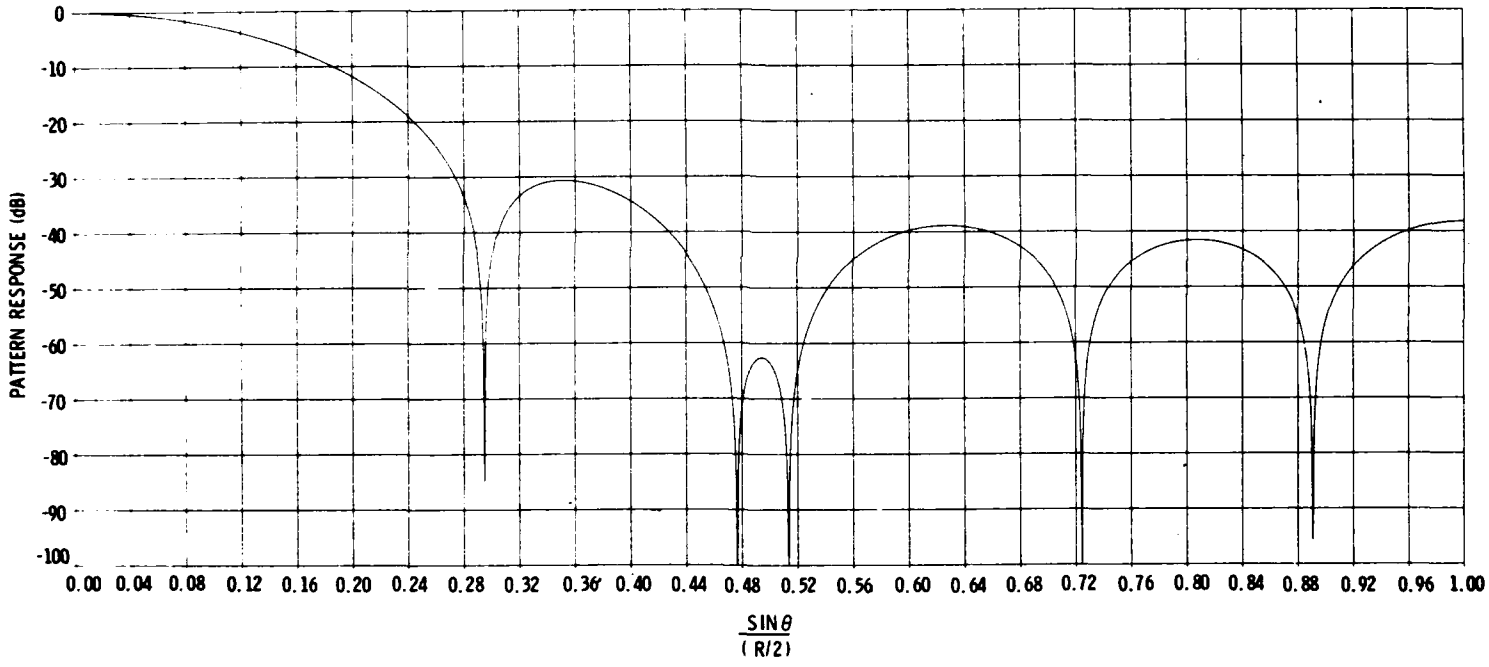

Figure 5-4. Pattern of J- Derived -25 dB Design Array (Level 9 Reference Array Sampled With Interval 163 and Truncated to 13 Elements)

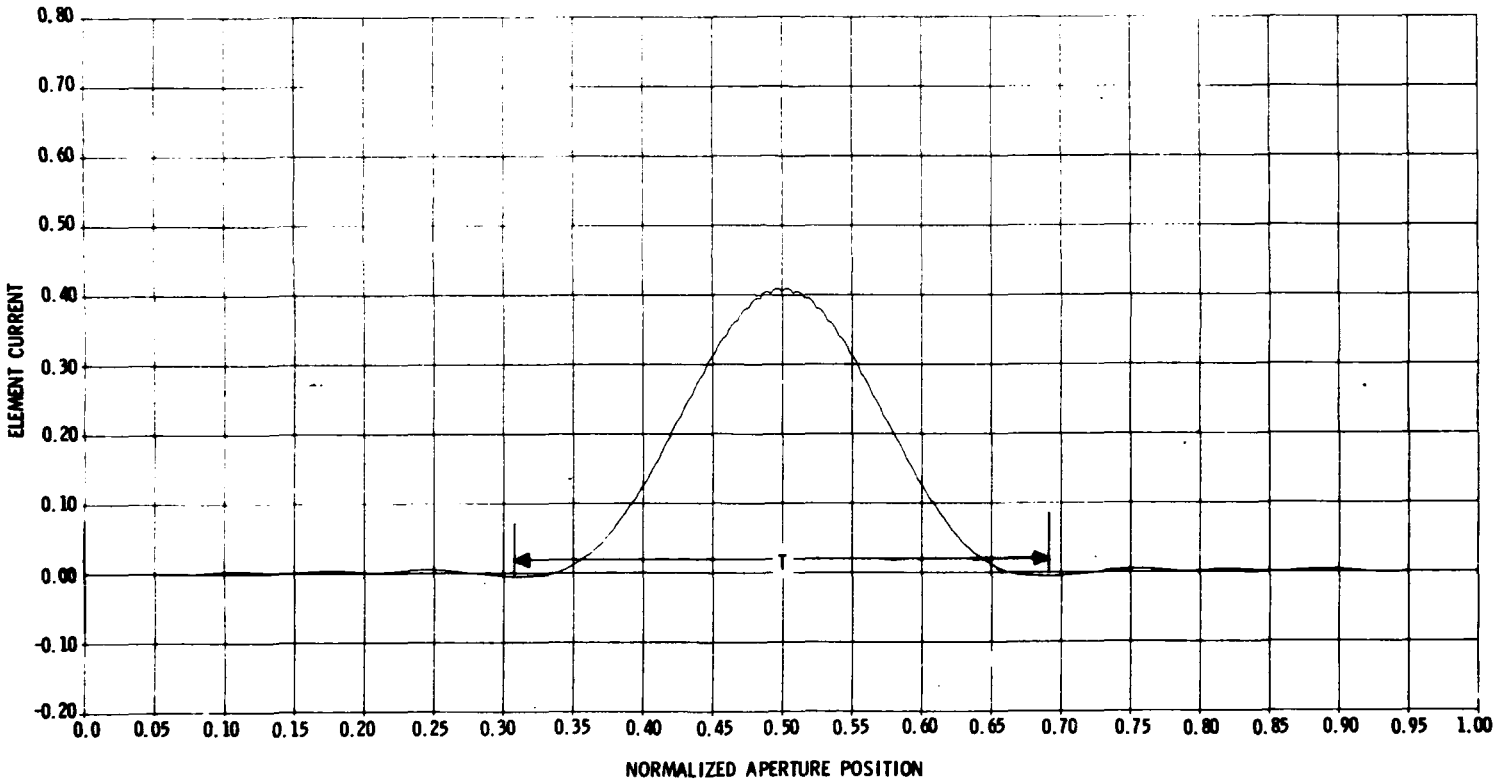

Figure 5-5. Current Distribution, -40 dB Design, 495 Points, L=5 (End Seeds at 0.4 and 0.6)

of Figure 5-6 results. Comparing with Figure 4-8 again reveals that truncation restores sidelobe levels to specification values. Keeping 47 out of 123 elements means that 76 of 123 or 62% of the reference array elements were removed.

Table 4-1 summarizes some of the data items involved in the pattern figures of this section.

The current distribution for the -50 dB design is shown in Figure 5-7. Selecting every 4^{th} element from this L=5 array yields the 171-element, L=3 array whose far-field pattern is shown in Figure 4-11. Truncation of this reference array to 55 elements produces the pattern shown in Figure 5-8. Comparison with Figure 4-11 shows a dramatic difference in sidelobe structure. Deletion of 116 elements out of 171 means that 68% of the reference array elements were discarded.

Routine use of these procedures yields an array having an odd number of elements. If an even number of elements is desired, the interpolation concept leads quickly to a simple procedure for odd-even conversion. One simply carries the design to an interpolation level one step beyond that originally intended. Then a 2:1 censoring is done such that the central element is not selected. An example of this procedure is shown in Figure 5-9 which may be compared directly with Figure 5-8.

Figure 5-10 shows the current distribution for the -65 dB design which contains 971 elements at level 5. The pattern of the level three array derived from this distribution is shown in Figure 4-12. When this array is truncated from 239 elements to 71, the pattern of Figure 5-11 results. Comparing this to Figure 4-12 shows that even though the peak sidelobe levels have been raised to the specification value, much of the remaining sidelobe region is suppressed far below the specification value. Retention of 71 of 239 elements means that 70% of the reference array was discarded by the truncation process.

It has been shown that this synthesis process results in current distributions that have desirable tapers. The direct (reference) array obtained from interpolation contains many elements at the edges with small weights. Truncation by use of an interactive computer program reduces the required aperture significantly while still maintaining prescribed sidelobe levels.

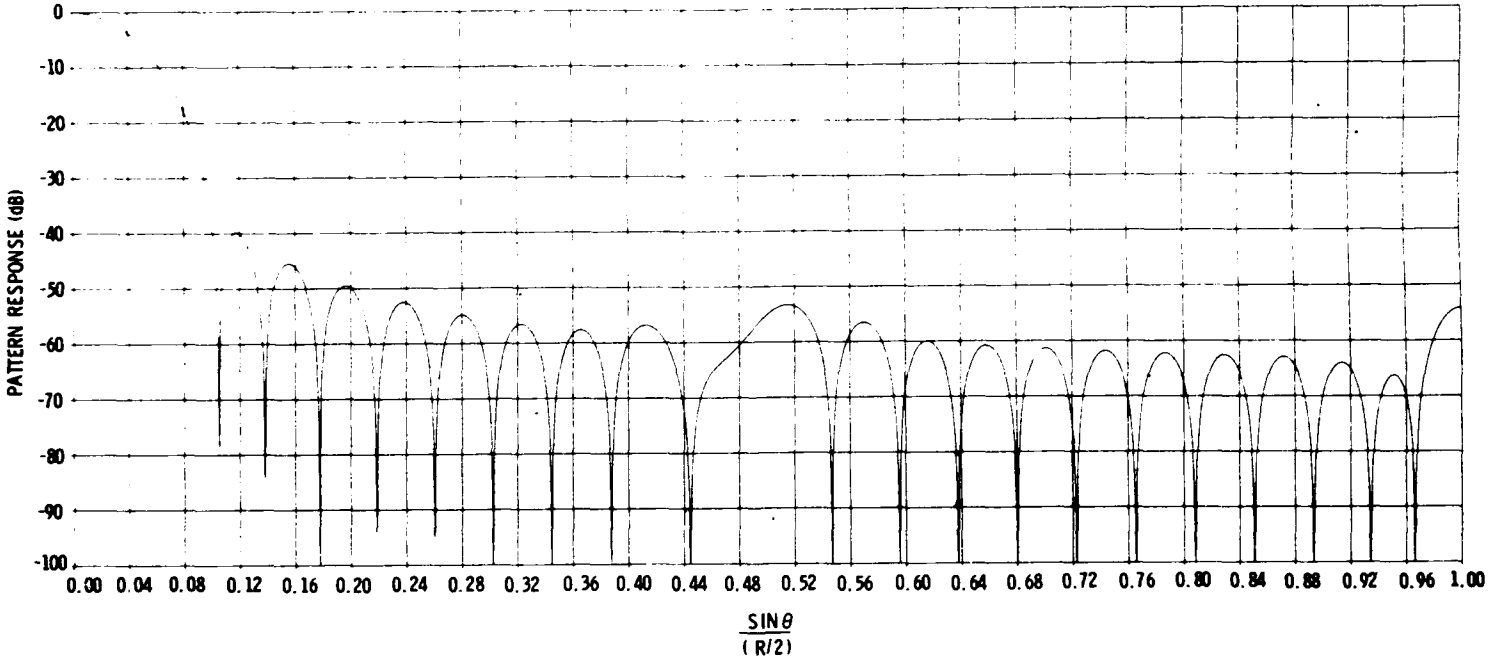

Figure 5-6. Pattern of -40 dB Design, Level 3 Array Truncated to 47 Elements from an Original 123

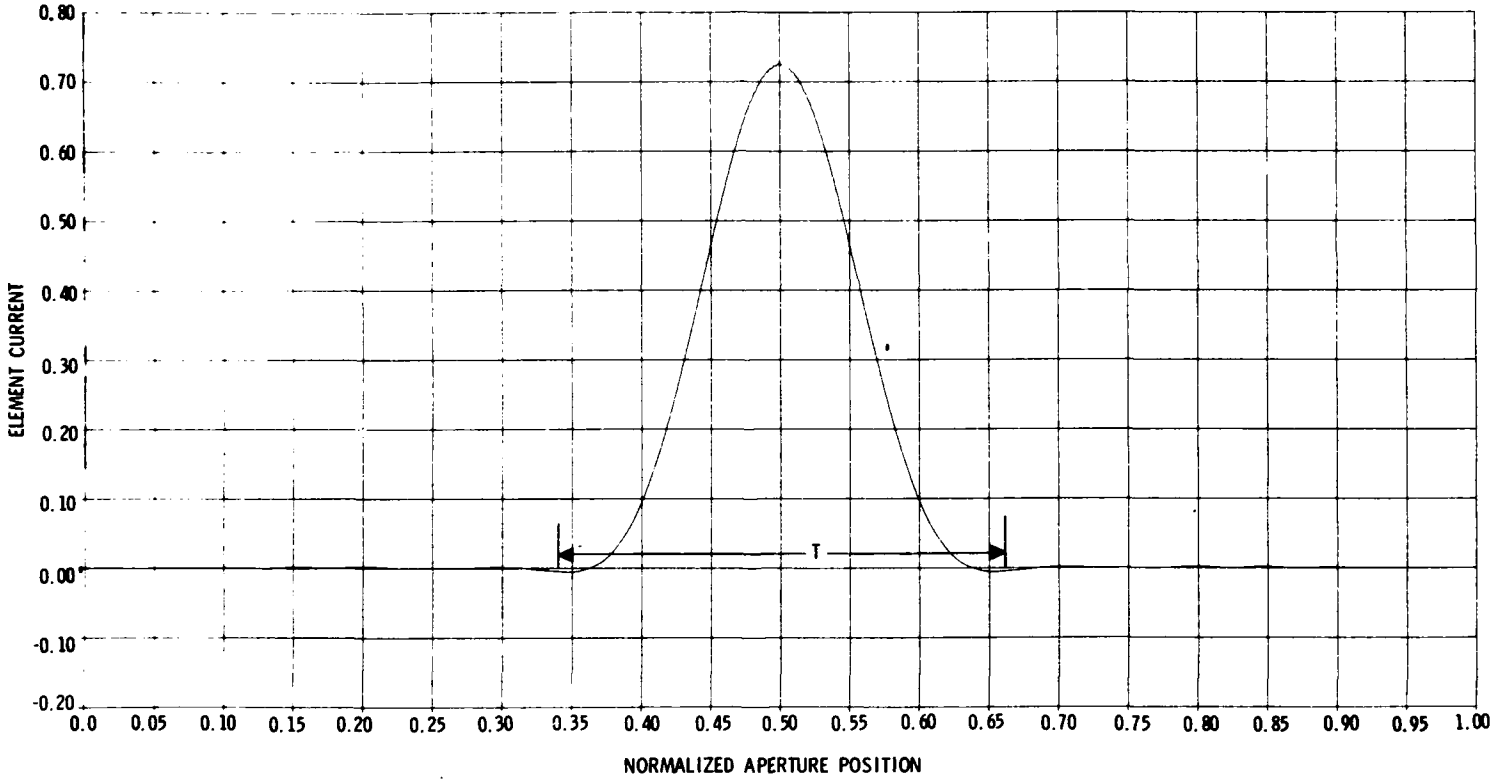

Figure 5-7. Current Distribution, -50 dB Design, 695 Points, L=5 (End Seeds at 0.41 and 0.59)

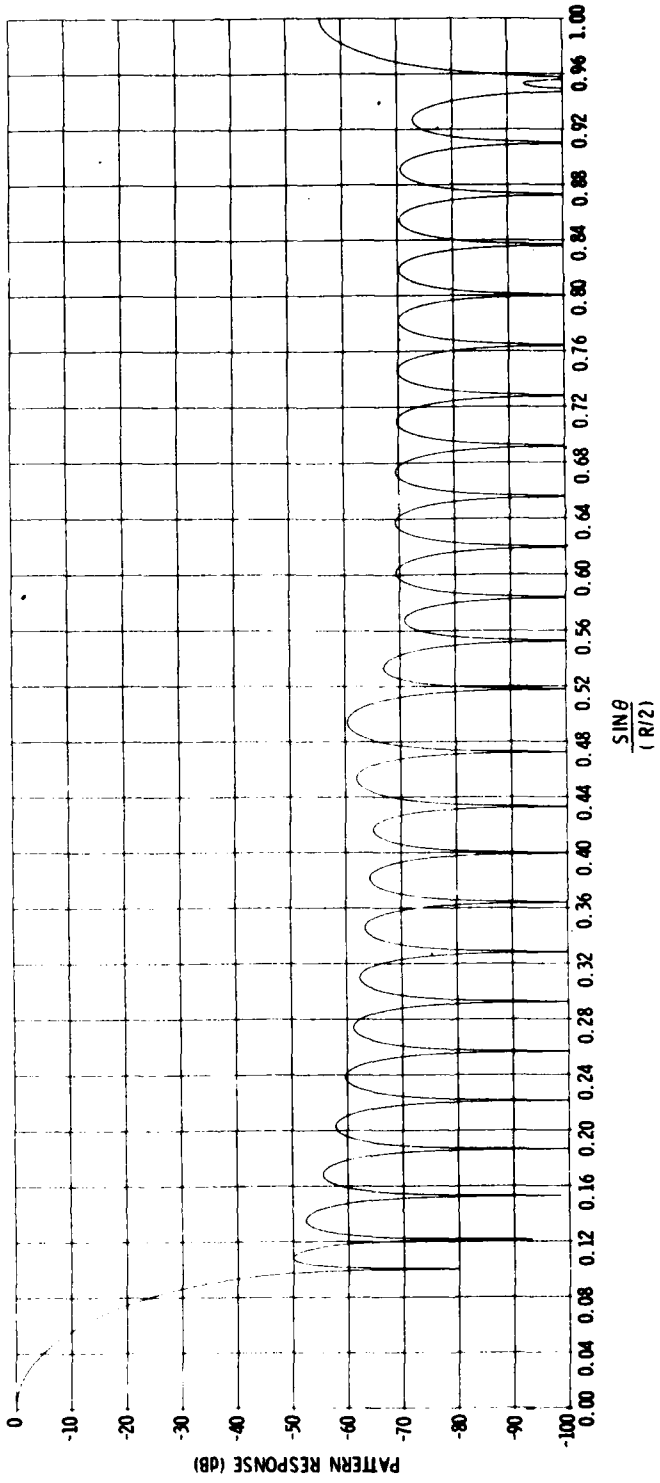

Figure 5-8. Pattern of -50 dB Design, Level 3 Array Truncated to 55 Elements from an Original 171

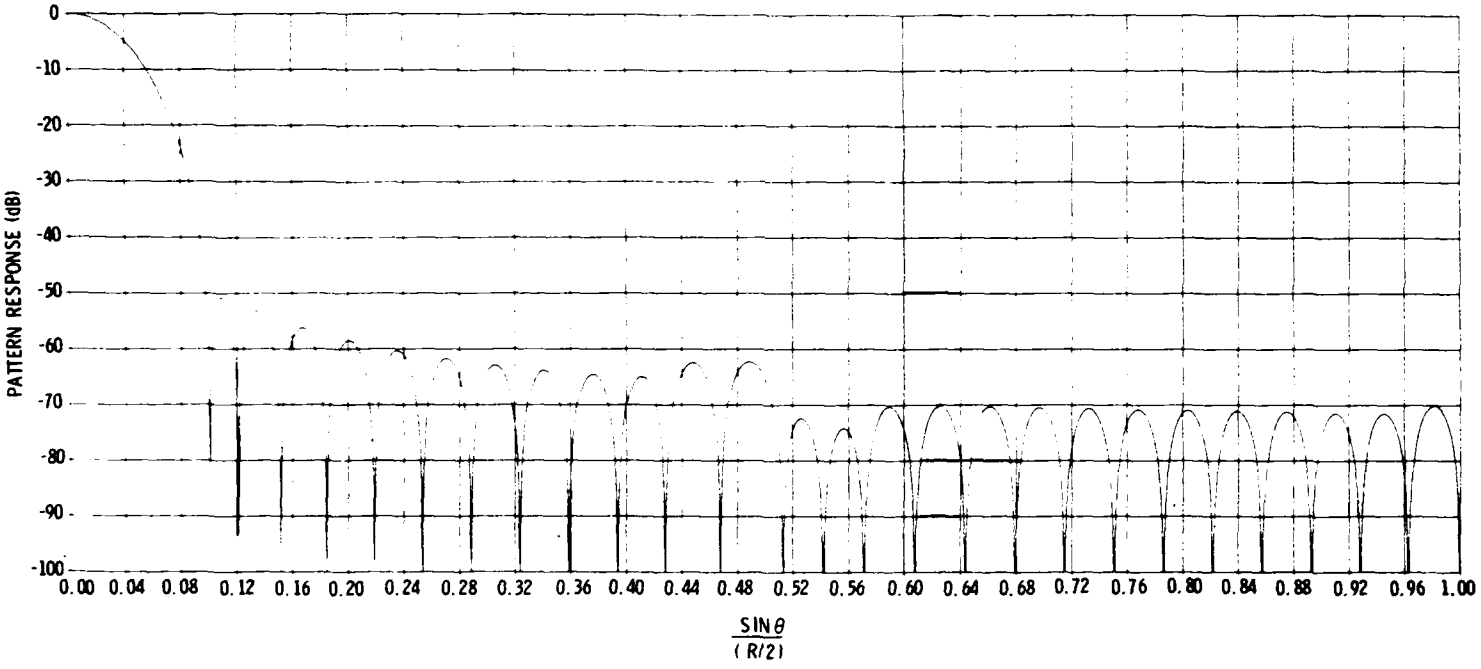

Figure 5-9. Pattern of 5-Element Seed After 4-Interpolation Levels, Truncation and Conversion to Even No. of Element Array (-50 dB Design). This Array Contains 56 Elements.

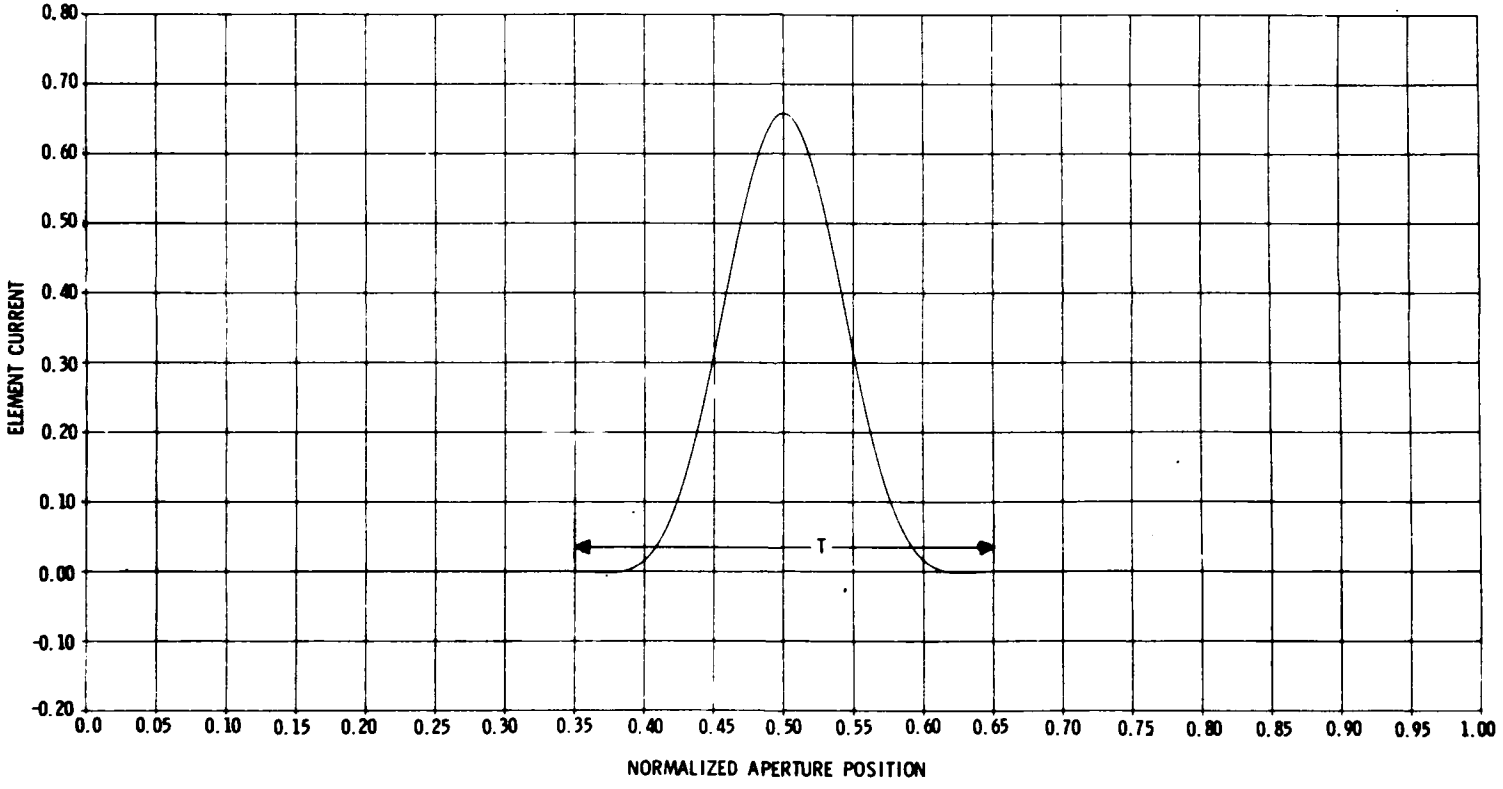

Figure 5-10. Current Distribution, -65 dB Design, 971 Points, L=5 (End Seeds at 0.42 and 0.58)

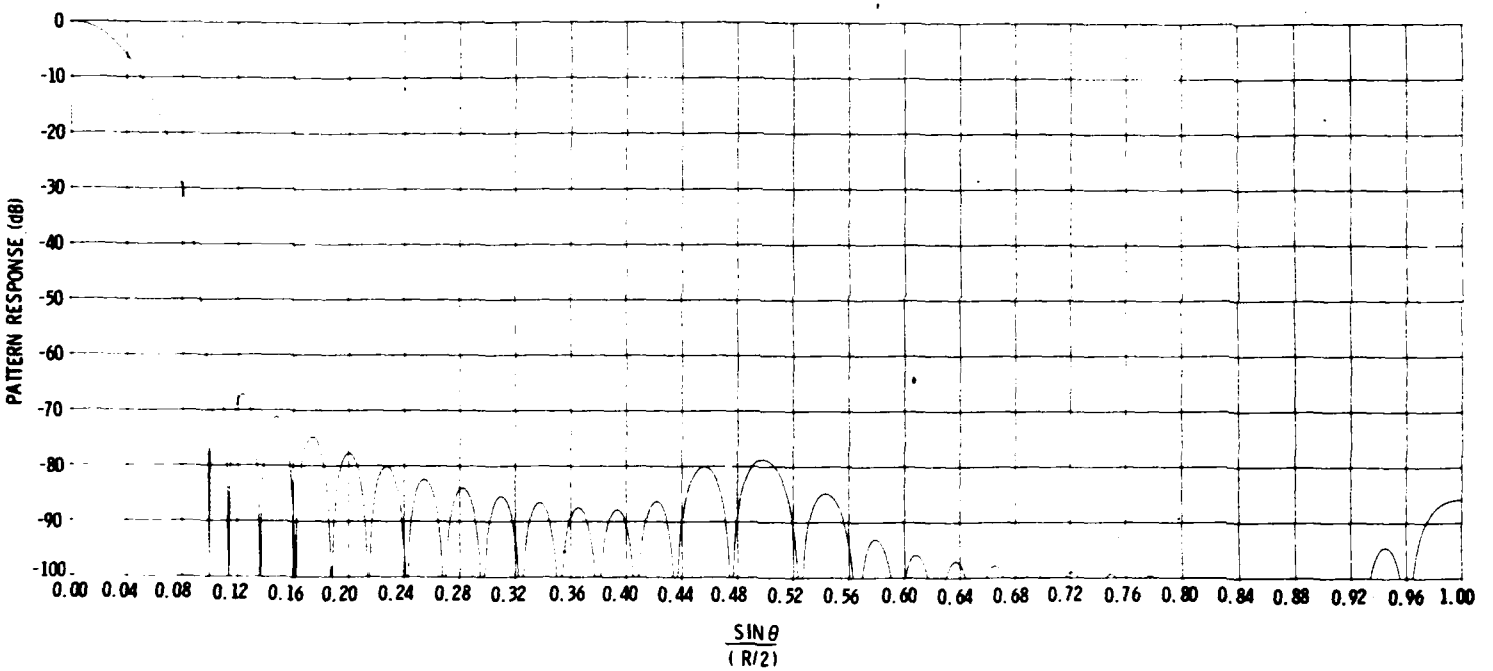

Figure 5-11. Pattern of -65 dB Design, Level 3 Array Truncated to 71 Elements from an Original 239

SECTION VI

STEERING AND FEED MATRIX ARCHITECTURE

Up to this point the problem of forming a beam pattern about $\theta = 0$ having prescribed properties has been considered. Attention has been paid to the number of elements needed and to the current values that must be applied to each element. In this section the previous work is extended to encompass the ability to steer the beam (shift the far-field pattern in $\sin\theta$ space) and means for creating the necessary aperture currents which produce the steered beam pattern are developed. A unique aperture illumination and feed matrix arrangement is described which accomplishes the beam steering function without the use of phase shifters. That is, the feed matrix operations are entirely real. The method is presented as a different approach to beam steering which gives to the array designer an additional option from which to choose.

An array is shown in Figure 6-1(a) having an odd number of elements with weights $\overline{W}_k$ and spacing between elements equal to T. For the moment ignore the interleaved array of elements which also has element spacing T and whose excitation values are indicated by g_k. Let the $\overline{W}_k$ array weights be derived, for example, from the work in Section V which would yield a symmetrically driven aperture with the beam center at $\theta = 0$. If these real weights are replaced by the complex weights $\hat{W}_k$

$$\hat{W}_k = W_k\, e^{-j2\pi k \frac{f_0}{R}} = W_k \cos 2\pi k \frac{f_0}{R} - j\, W_k \sin 2\pi k \frac{f_0}{R} \tag{6-1}$$

The far-field pattern becomes

$$E(f) = W_0 + \sum_{k=1} \hat{W}_k\, e^{+j2\pi k \frac{f}{R}} + \sum_{k=1} \hat{W}_{-k}\, e^{-j2\pi k \frac{f}{R}} \tag{6-2}$$

$$E(f) \quad W_0 + \sum_{k\ 1} W_k\, e^{+j2\pi k \frac{(f-f_0)}{R}} + \sum_{k\ 1} W_{-k}\, e^{-j2\pi k \frac{(f-f_0)}{R}} \tag{6-3}$$

Since $W_k = W_{-k}$ there results

$$E(f) \quad W_0 + \sum_{k\ 1} 2W_k \cos 2\pi k \frac{(f-f_0)}{R} \tag{6-4}$$

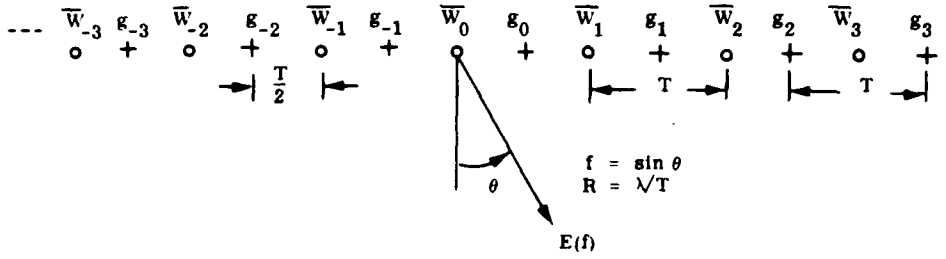

(a) Interleaved Aperture

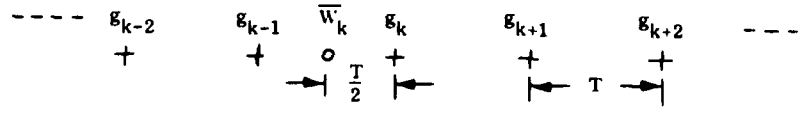

(b) Quadrature Current Substitution Details

Figure 6-1. Array and Feed Matrix (Sheet 1 of 2)

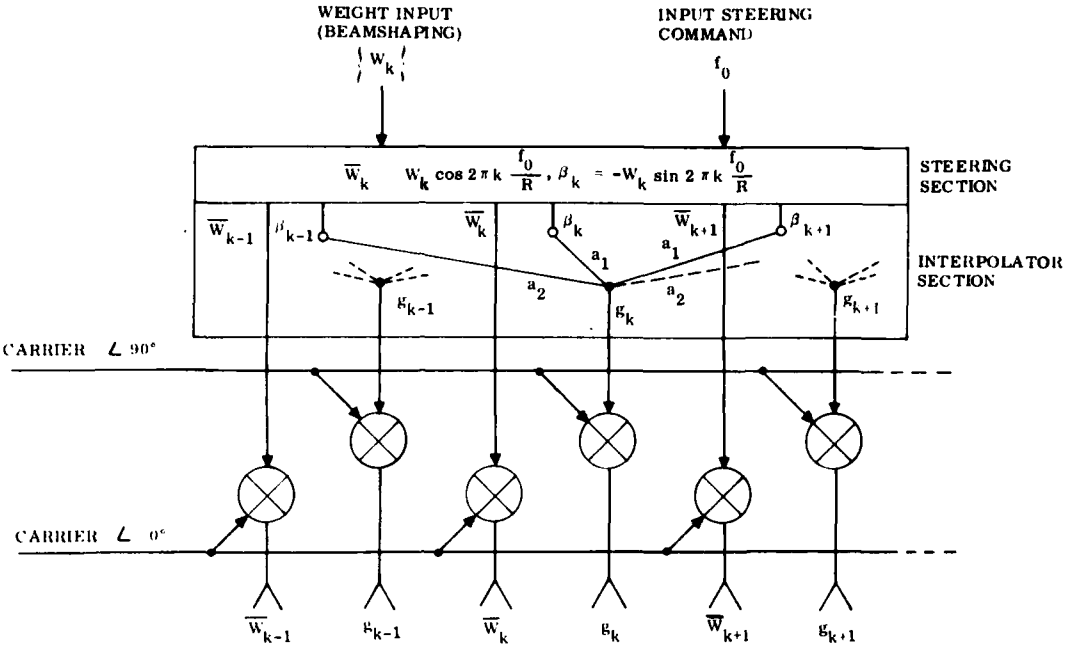

(c) Feed Matrix and Element Drive Modules

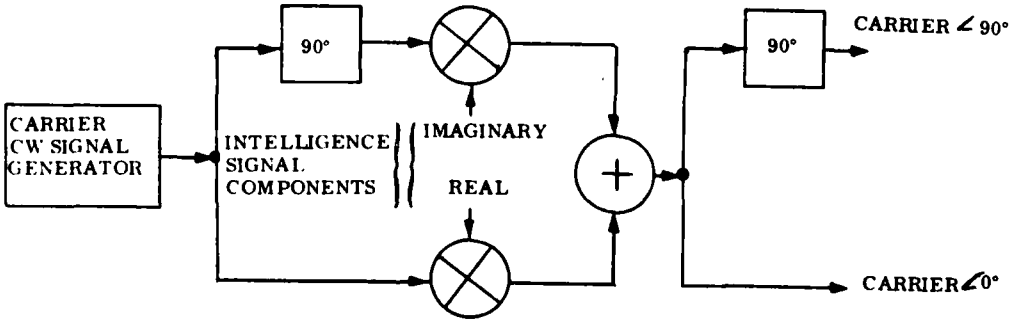

(d) Carrier Signal Generation

Figure 6-1. Array and Feed Matrix (Sheet 2 of 2)

If E_0 (f) is defined as the far-field pattern existing from real weights ($f_0 = 0$) then

$$E(f) = E_0 (f - f_0) \tag{6-5}$$

and steering has been accomplished.

The E(f) pattern is real and is generated in part by the real excitation currents and in part by the quadrature or imaginary excitation currents of Equation (6-1). The corresponding components of the far field are given by

$$E_R(f) = W_0 + \sum_{k=1} W_k \left[\cos 2\pi k \frac{(f - f_0)}{R} + \cos 2\pi k \frac{(f + f_0)}{R} \right] \tag{6-6}$$

and

$$E_I(f) \sum_{k=1} W_k \left[\cos 2\pi k \frac{(f - f_0)}{R} - \cos 2\pi k \frac{(f + f_0)}{R} \right] \tag{6-7}$$

where

$$E(f) = E_R(f) + E_I(f) \tag{6-8}$$

The real currents produce a pair of symmetrically shifted, real beams at $f - f_0$ and $f + f_0$. The imaginary currents do precisely the same thing except for a polarity reversal in the left-shifted pattern which provides for the cancellation of the "image" beam and reinforces the beam steered to $f = f_0$.

Beam steering clearly requires the effects of complex currents at the elements and it is normal practice to employ phase shifters in excitation matrices of beamsteering phased arrays. We propose here to eliminate the need for phase shifters by utilizing a pair of interleaved arrays, each fed with currents of one phase only. The $\overline{W}_k$ set of Figure 6-1(a) will be fed entirely with real or 0° phase currents, while the g_k set will be fed with imaginary or 90° phase currents. Polarity reversals in both sets due to negative real weights will be allowed. The currents in the $\overline{W}_k$ set will be, by our option, the real component of $\overline{W}_k$ of Equation (6-1)

$$\overline{W}_k = W_k \cos 2\pi k \frac{f_0}{R} \tag{6-9}$$

The imaginary component of current formerly at $\overline{W}_k$

$$q_k = -j W_k \sin 2\pi k \frac{f_0}{R} \tag{6-10}$$

has been omitted. An attempt will be made to excite nearby g_k elements so that the far-field will be unaware of the transfer of quadrature current from $\overline{W}_k$ to its quadrature-excited neighbors. This cannot be done exactly, but as will be seen, it can be done with sufficient accuracy in a practical manner if proper interpolation procedures are followed.

All quadrature currents must have an odd-symmetric counterpart in the array since the far-field pattern is to be maintained real. A unit quadrature current (+j) at distance x from array center (along with its counterpart) produces a far-field phasor

$$E_j = -2 \sin 2\pi x \frac{f}{\lambda} \tag{6-11}$$

The field of the original quadrature current of Equation (6-10) is then

$$E_{q_k}(f) = 2 W_k \sin 2\pi k \frac{f_0}{R} \sin 2\pi k \frac{f}{R} \tag{6-12}$$

which becomes the target of the approximation process which follows.

The far-field pattern of Equation (6-12) will be synthesized by N pairs of symmetrically excited elements $(g_k = g_{k-1})$, $(g_{k+1} = g_{k-2})$, --, $(g_{k+N-1} = g_{k-N})$ etc. as detailed in Figure 6-1(b). The far-field pattern of these N pairs (and their odd-symmetric counterparts) is given by

$$A_k(f) = \left\{ \sum_{n=1}^{N} -4 g_{k+n-1} \cos 2\pi \frac{(2n-1)}{2} \frac{f}{R} \right\} \sin 2\pi k \frac{f}{R} \tag{6-13}$$

Now it is desired that $A_k(f)$ of Equation (6-13) agree as closely as possible with $E_{q_k}(f)$ of Equation (6-12), an identity is not possible so we write

$$\sum_{n=1}^{N} -4 g_{k+n-1} \cos 2\pi \frac{(2n-1)}{2} \frac{f}{R} \approx 2 W_k \sin 2\pi k \frac{f_0}{R} . \tag{6-14}$$

For any given k value and steering angle f_0, the right-hand side is a constant (W_k is also prespecified). For illustrative purposes we normalize by defining

$$2a_n \quad b_n \quad \frac{-2 g_{k+n-1}}{W_k \sin 2\pi k \frac{f_0}{R}} . \tag{6-15}$$

then Equation (6-14) may be written in the familiar form of

$$H(f) = \sum_{n=1}^{N} b_n \cos 2\pi \frac{(2n-1)}{2} \frac{f}{R} \cong 1 \qquad (6\text{-}16)$$

which is H(f) of Equation (1-3).

A set of coefficients b_n can be found which will hold the approximation of Equation (6-16) to within a specified error out to a design cutoff of $f = \gamma R/2$ as extensively discussed in previous sections.

Suppose now that an a_n, b_n set is selected. The g-values required in the W_k neighborhood would be given by, (using Equation 6-15)

$$g_{k+n-1} = a_n \left(-W_k \sin 2\pi k \frac{f_0}{R} \right), \quad n = 1, 2, \text{---} N \qquad (6\text{-}17)$$

which would yield (g_k, g_{k-1}), (g_{k+1}, g_{k-2}), -- (g_{k+N-1}, g_{k-N}) because of the assumed symmetry. Thus the single computed value $(-W_k \sin 2\pi k f_0/R)$ contributes to 2N g-values through the a_n weights. Worked the other way around, this means that each g-element of the array will be fed from 2N of the q_k "missing currents" of Equation (6-10). Thus, the expression for the g-currents becomes

$$g_k = \sum_{n=1}^{N} a_n \left[-W_{k+n} \sin 2\pi (k+n) \frac{f_0}{R} - W_{k+1-n} \sin 2\pi (k+1-n) \frac{f_0}{R} \right] \qquad (6\text{-}18)$$

which, not surprisingly, amounts to an interpolation process over a neighboring set of "missing" quadrature currents (see Equation (6-10)). The real currents are available without ceremony from the simple calculation of Equation (6-9) and are used to feed the original $\overline{W_k}$ elements as described before.

It is interesting to note that this process of converting a set of array samples requiring complex operations for their generation to a set of array samples permitting real operations in their generation is identical to a signal processing procedure treated earlier by the writer [Ref. 1, Sections 5.1, 5.2, see especially Equation (4-4)] . In fact the computer program needed to implement conveniently the feed matrix of Figure 6-1(c) is available [Ref 1, Section 6.1, subroutine CORE, complex-to-real transformation] .

(In signal processing work sampled data is usually found in one of two formats. A bandpass signal may be downshifted to a low (baseband) frequency, and this translated version is sampled to yield "real samples". Alternately a cosine and sine detection near band-center of the signal may be done and the resulting lowpass I and Q-components may then be

sampled to yield "complex samples". It often occurs in signal processing work that transformations from one sampling format to the other are required. It was shown in the reference previously cited that these transformations are in reality interpolation problems. Subroutines for complex-to-real (CORE) and real-to-complex (RECO) conversions are presented and described in the previous reference.)

A few comments now on the synthesis of the required odd-symmetric far field by the g_k set as described in Equations (6-13 through 6-16). Equations (6-6 and 6-7) show that failure to produce $E_I(f)$ will leave the $f+f_0$ portion of $E_k(f)$ uncancelled and an "image" beam will appear. Substitution of Equation (6-17) into Equation (6-13) yields, using also Equations (6-16 and 6-7),

$$A_k(f) \quad H(f)\ 2\,W_k \sin 2\pi k \frac{f_0}{R} \sin 2\pi k \frac{f}{R} \tag{6-19}$$

and therefore

$$\sum_k A_k(f) \quad H(f) \sum_k W_k \left[\cos 2\pi k \frac{f - f_0}{R} - \cos 2\pi k \frac{f+f_0}{R}\right] = H(f)\ E_I(f) \tag{6-20}$$

When this is compared to Equations (6-12) and (6-7) it will be seen that the surrogate quadrature currents are doing exactly the right thing except for level (amplitude) errors. From f = 0 to f = $\gamma R/2$ H(f) has a maximum error (deviation from unity) of $\pm\ \delta$ as discussed in Section I. For $f > \gamma R/2$, H(f) ceases its valiant struggle for unity and quietly goes to zero at f = R/2. The region beyond $f = \gamma R/2$ will be an errored region in which the $E_R(f)$ of Equation (6-6) will prevail undiminished while the g_k set will only be able to supply a fraction of the $E_I(f)$ of Equation (6-7). Real harm will occur in such cases only if the beam is steered to an f value in ($\gamma R/2$, R/2) or ($-\gamma R/2$, -R/2). The true main beam may appear somewhat distorted in the process, but an uncancelled image will appear at the other f-space extremity. The failure of the image to cancel cannot be tolerated. Steering to $\pm$ R/2 represents an ultimate, obviously. Interplators that will give us 80% to 90% of this space are readily available. The main price paid for higher γ is (usually) a modest extension of aperture.

In the working region ($-\gamma R/2 < f < \gamma R/2$) the failure of the g_k set to cancel the image main beam will, in essence, tend to violate the sidelobe specification for the array. The Figure 6-1 interpolator must therefore have a stopband specification at least equal to the sidelobe level desired.

These matters are demonstrated in Figures 6-2 through 6-8. The feed matrix of Figure 6-1(c) was programmed using the signal-processing subroutine CORE (the polarity

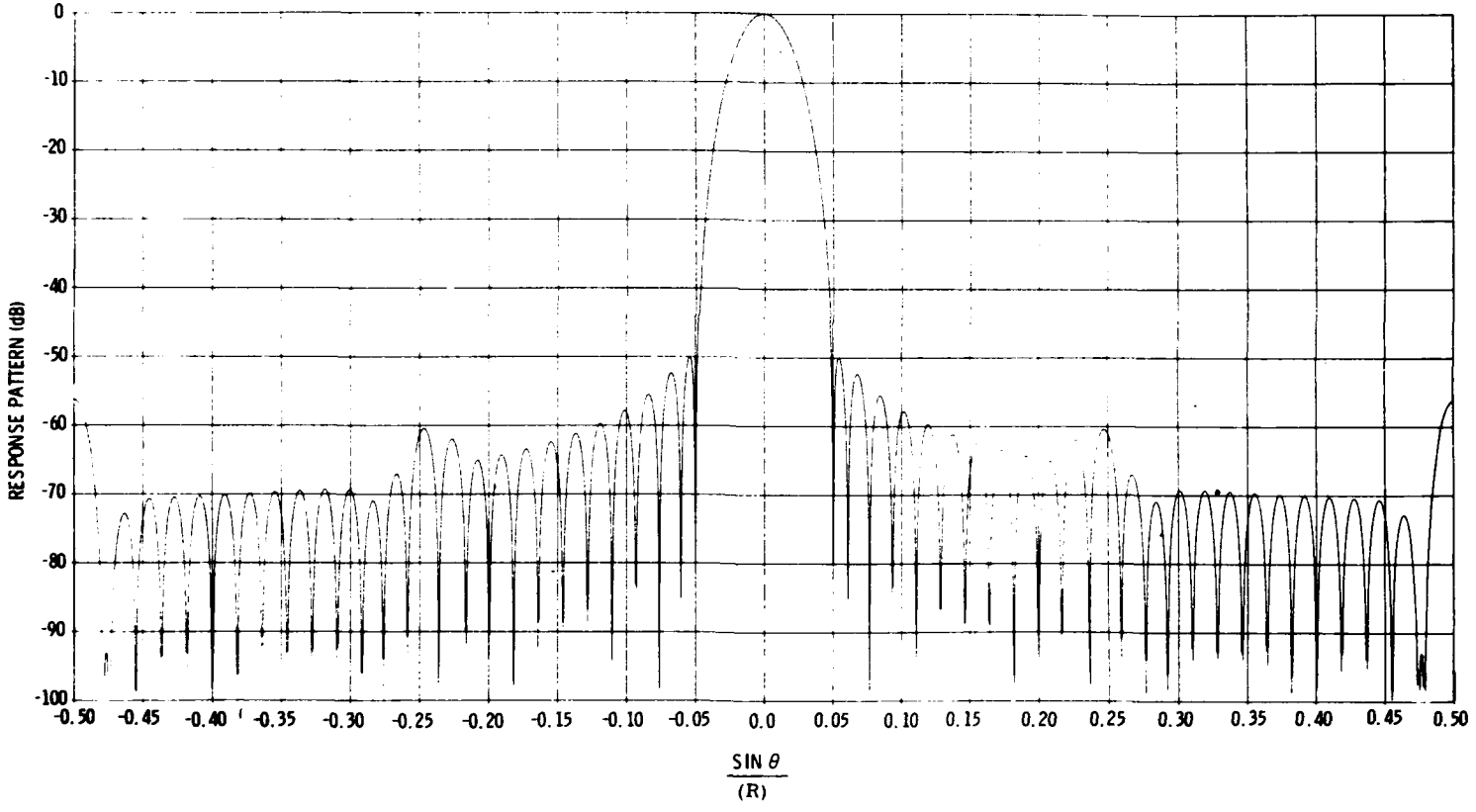

Figure 6-2. Reference (Unsteered) Pattern. Same as Pattern of Figure 5-8. Beam Steering Interpolator, NT = 2 (-50 dB, $\gamma = 0.8$)

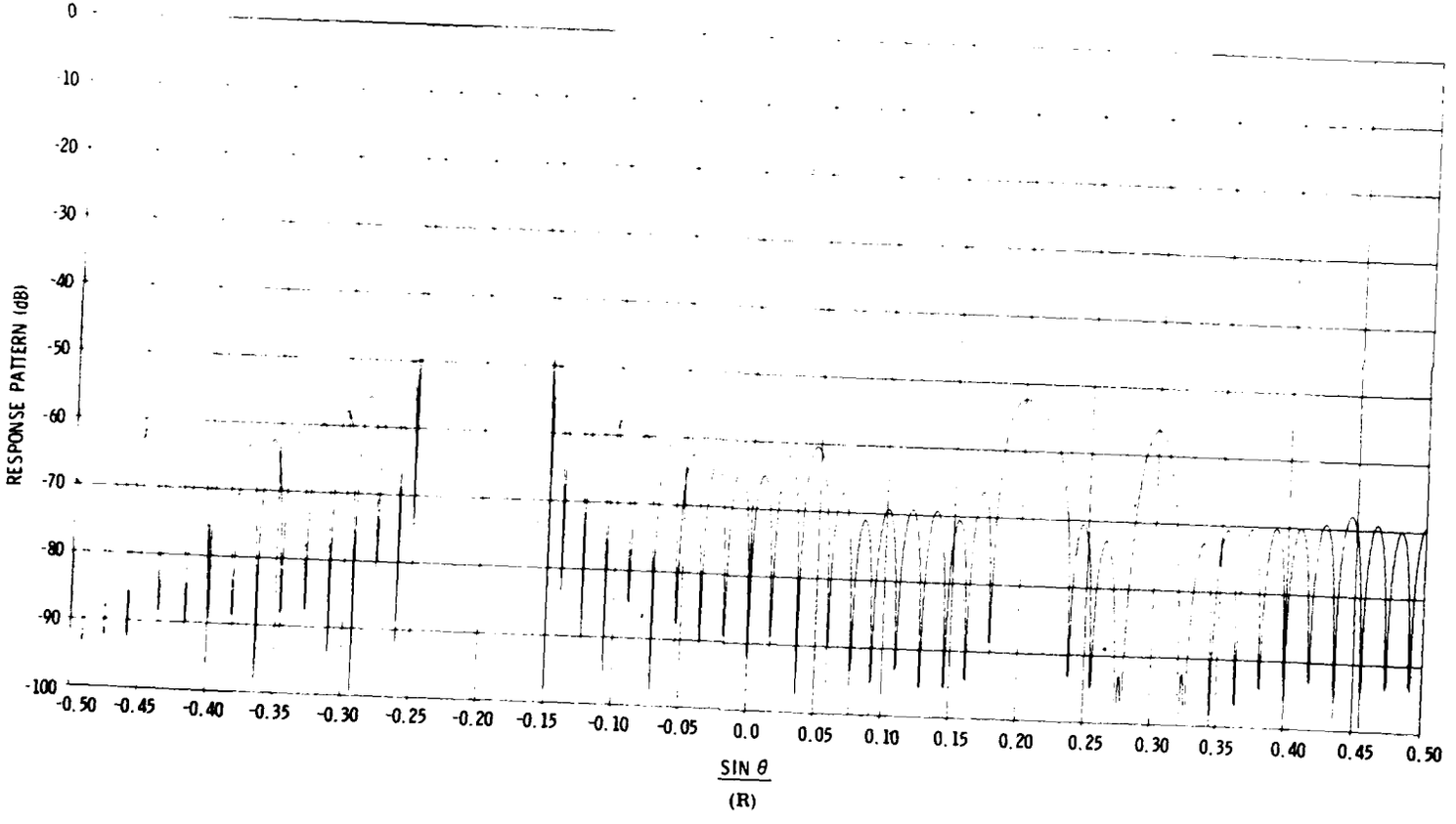

Figure 6-3. Reference Pattern Steered to -0.2R. Beam Steering Interpolator, NT = 2 (-50 dB, $\gamma = 0.8$)

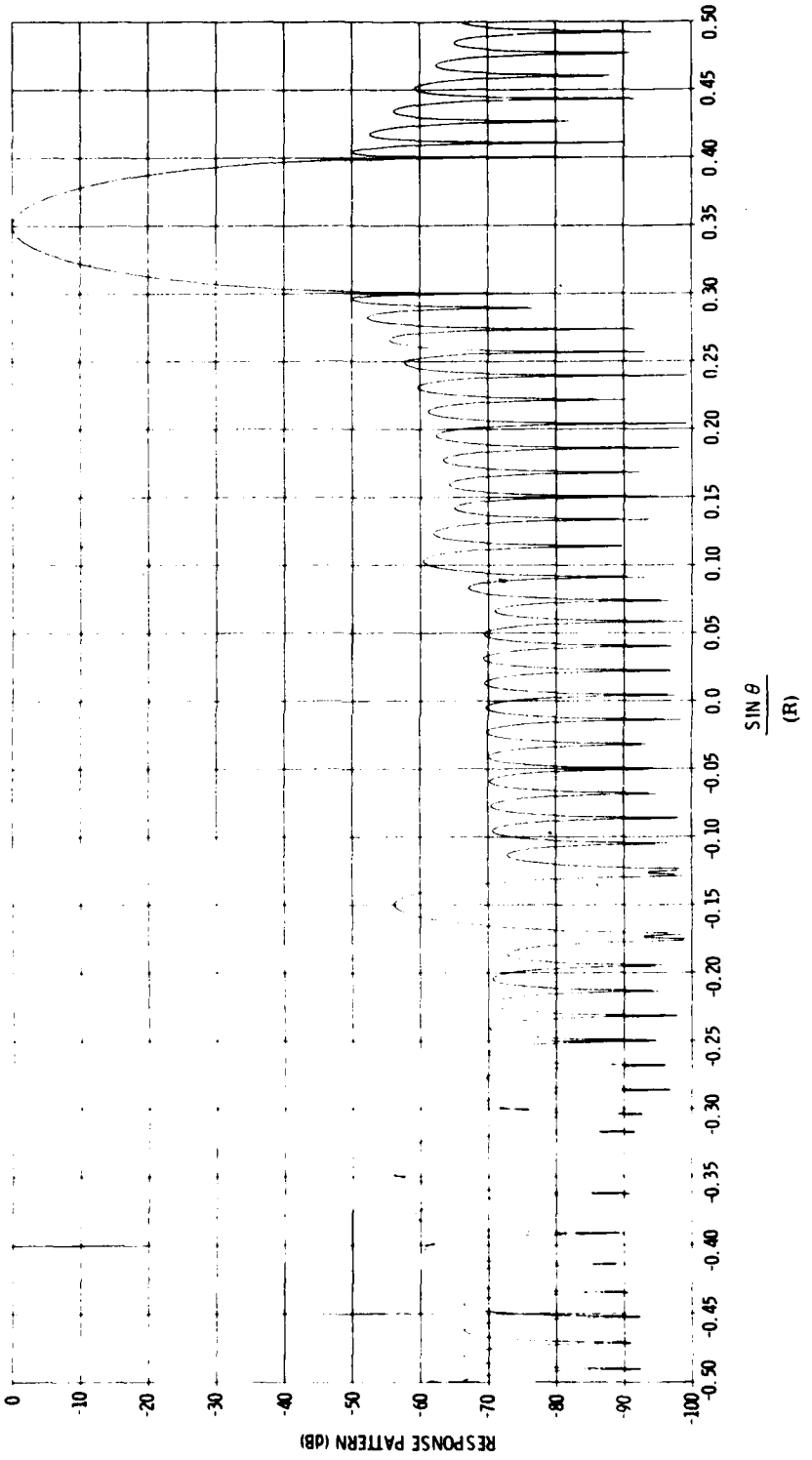

Figure 6-4. Reference Pattern Steered to +0.35R. Beam Steering Interpolator, NT = 2 (-50 dB, $\gamma = 0.8$)

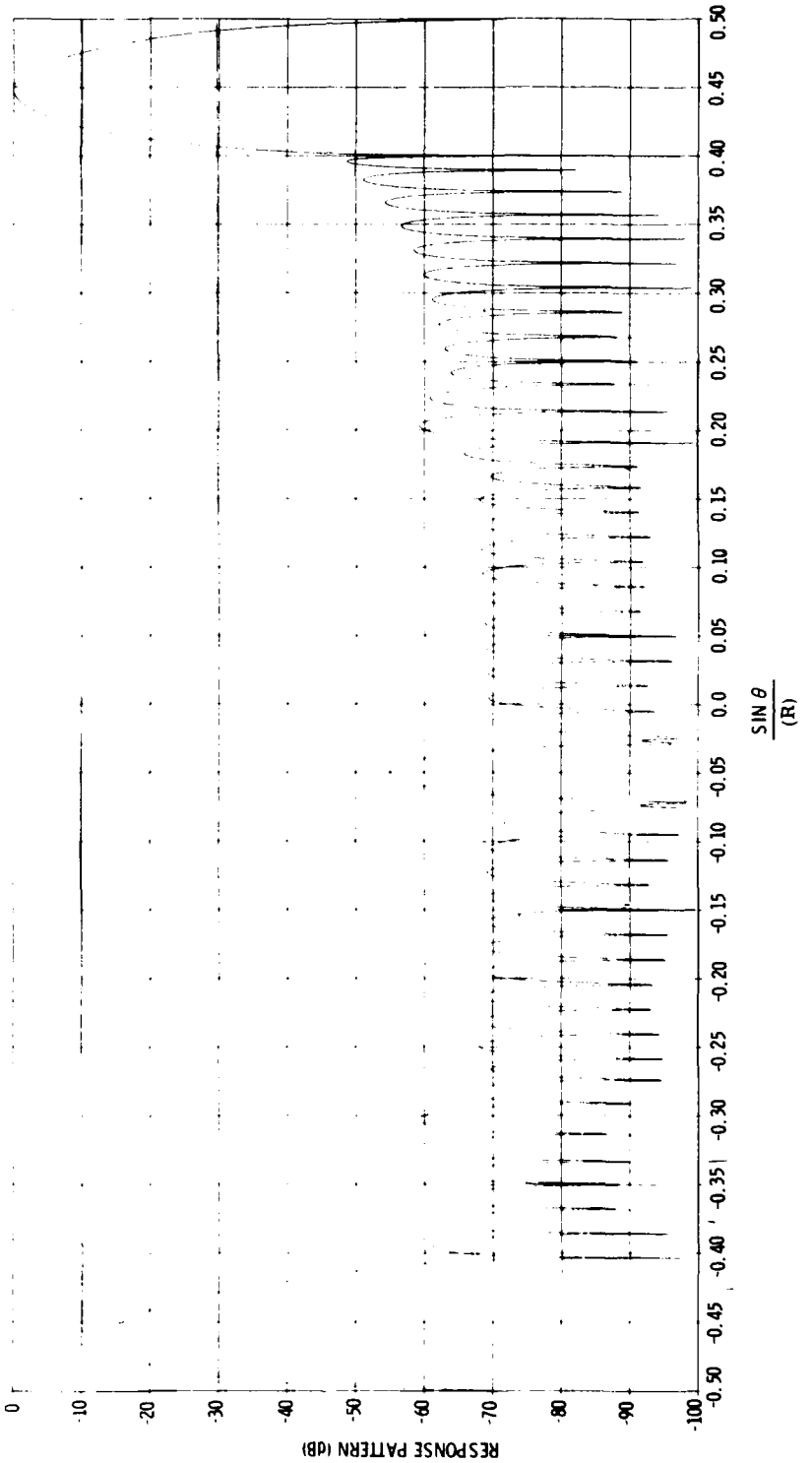

Figure 6-5. Reference Pattern Steered to +0.45R, Beam Steering Interpolator, NT = 2 (-50 dB, $\gamma = 0.8$)

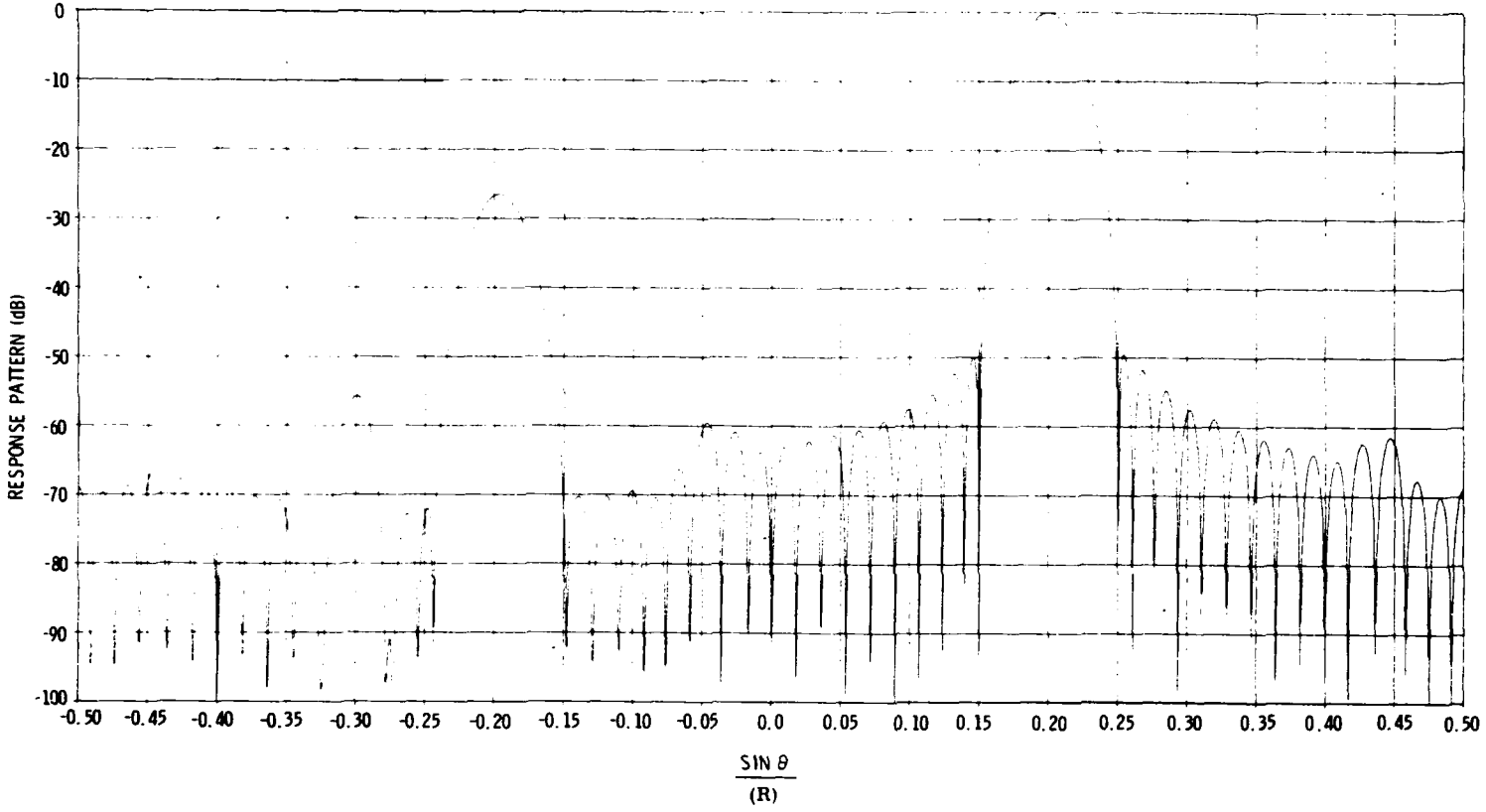

Figure 6-6. Reference Pattern Steered to +0.2R. Beam Steering Interpolator, NT = 4 (-25 dB, $\gamma = 0.8$)

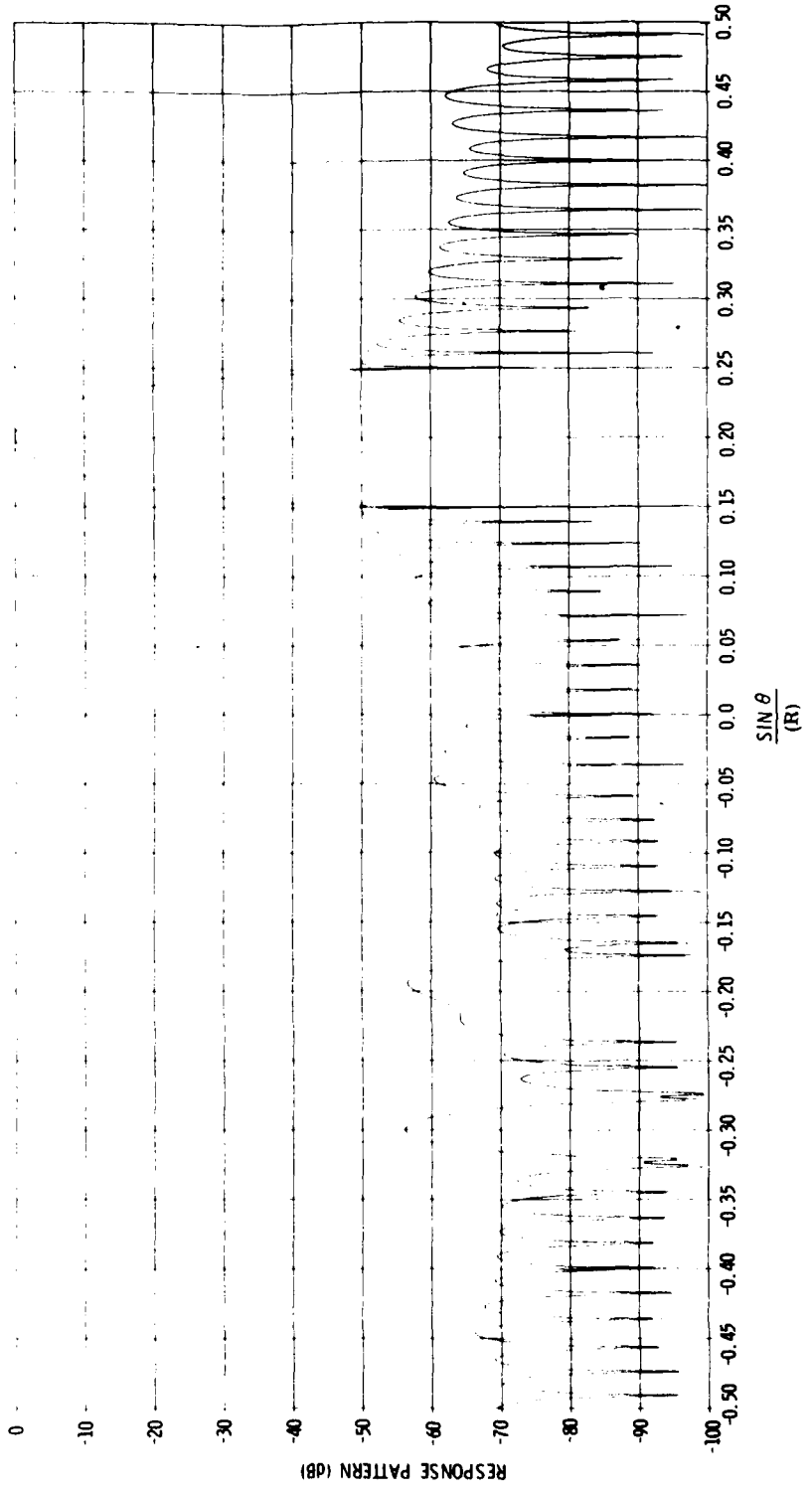

Figure 6-7. Reference Pattern Steered to +0.2R. Beam Steering Interpolator, NT = 10 (-50 dB, $\gamma = 0.6$)

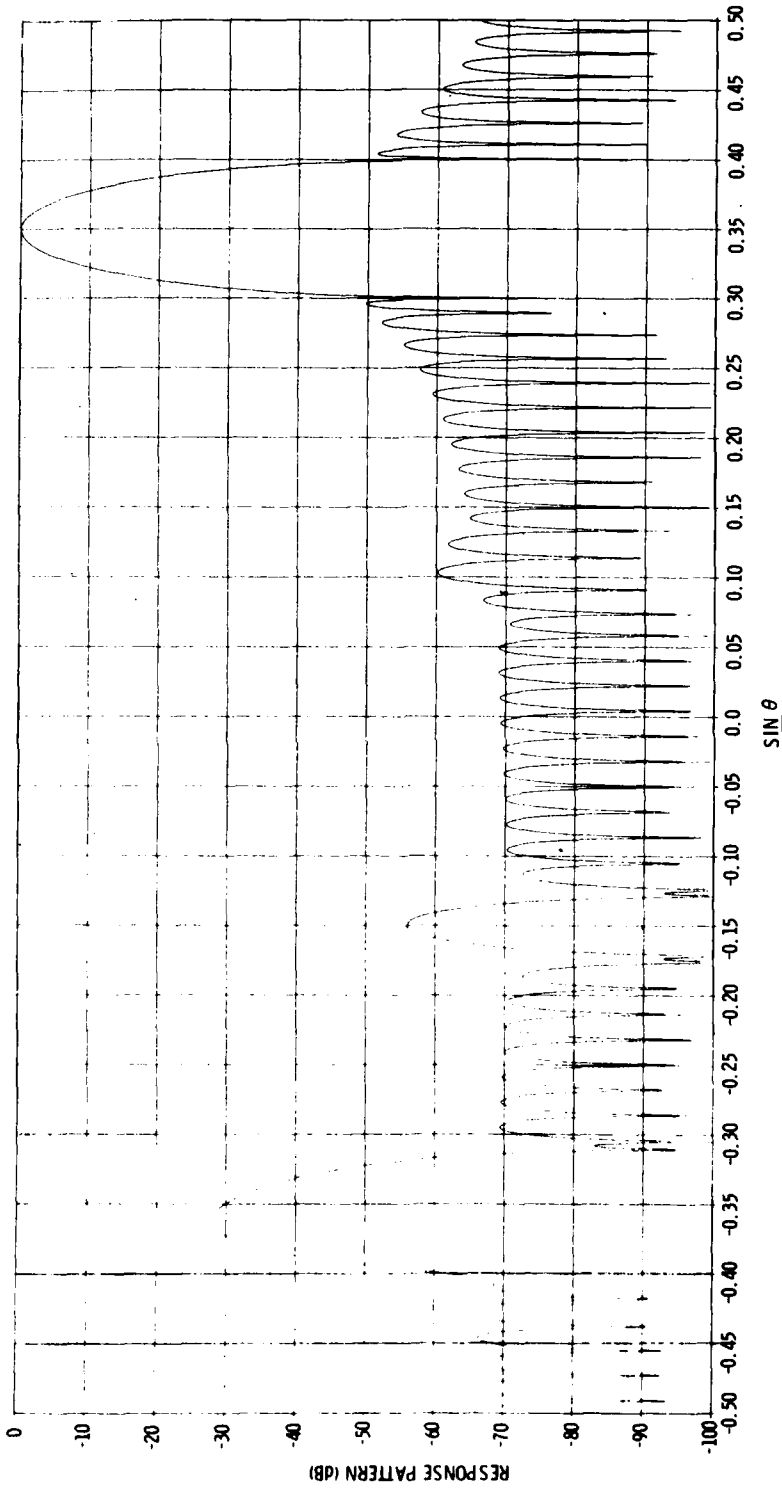

Figure 6-8. Reference Pattern Steered to +0.35R. Beam Steering Interpolator, NT = 10 (-50 dB, $\gamma = 0.6$)

reversals provided by CORE [Ref 1, Appendix A] must be eliminated for this use) for implementation of the interpolator section of Figure 6-1(c) as previously discussed. The reference pattern chosen for this group of examples was the -50 dB pattern of Figure 5-8. This 55-element pattern was chosen because the low sidelobe levels would make immediately obvious any performance deviations of the feed matrix. As will be seen the structure of Figure 6-1(c) performs exactly as advertised.

Figure 6-2 shows the reference pattern of Figure 5-8 in the plotting format of this group. The beam is centered in the broadside direction with f = ±R/2 at the plot extremities. Thus, these plots show an entire far-field period. The -55 dB sidelobe at f = ±R/2 should be noted. With f_0 set to zero, it follows from Figure 6-1(c) that all the g_k currents are zero, while the $\overline{W}_k$ currents equal the original W_k weights. Thus the array is restored exactly to the unsteered format analyzed in Section V.

Figure 6-3 shows steering for f_0 = -0.2R. The -55 dB sidelobe has moved down from f 0.5R to f - 0.3R. Note the "image" of the main lobe at f = +0.2R. The beam steering interpolator is the NT = 2 choice which provides a stopband attenuation of about -50 dB. This is well demonstrated by the "sidelobe" response at f = +0.2R. Comparing these last two figures shows that in all major features a pattern rotation has indeed been implemented by the feed matrix.

The beamsteering interpolator γ of 0.8 at NT = 2 indicates that the f_0 operating region of the matrix extends to ±0.8 x 0.5R = ±0.4R. Figure 6-4 shows steering to f_0 = +0.35R. The -55 dB sidelobe has moved from -0.5R to -0.15R and the "image" of the main beam at f - -0.35R is clearly evident. (The shape of the image will change depending upon its exact location within the H(f) pattern.) The pattern shown here near the design edge of the matrix is proper and correct.

Figure 6-5 shows steering beyond the design limits to f_0 = +0.45R. In this region the surrogate quadrature currents can no longer produce the properly-sized, far-field contribution. The main lobe loses some level (not noticeable with plot normalization). The main effect however appears in the image region in which two relatively large pattern components can no longer produce the small difference which was held to a level below -50 dB in the operating region. The "sidelobe" level observed here is of the order of -14 dB. This is a rather clear indication of a serious deviation from the norm.

In Figure 6-6 the beam steering interpolator is changed to an NT = 4 design which has a γ of 0.8 but only a -25 dB stopband specification. The "image" beam at f = 0.2R in response to the main beam at f_0 = +0.2R clearly shows the design mismatch. With the exception of this rather serious lapse, the remainder of the pattern of Figure 6-6 is quite satisfactory.

Figures 6-7 and 6-8 use a beam steering interpolator choice of NT = 10 which has a -50 dB stopband design but a γ of only 0.6. Thus the operating limits here on f_0 are $\pm 0.6 \times .5R = \pm 0.3R$. Figure 6-7 shows the pattern for a pointing angle of $f_0 = +0.2R$. Normal operation results with the image beam well below the -50 dB specification level.

Figure 6-8 shows the same beamformer steered to +0.35R, which is beyond the ±0.3R design limit. As expected, the problem area is at f = -0.35R where a -28 dB image beam appears.

These examples confirm the design philosophy which led to the design of the feed matrix of Figure 6-1(c). The extension of aperture needed to accomodate the interleaved elements has been of the order of 20% for the data shown. These are raw, untruncated results and should not be given any special significance. Quick looks at the element-weight listings indicate that considerable truncation may be done as was the case in Section V. An estimate of the aperture extension required for the above cases might be 5 to 10%. This matter will be more thoroughly studied when time and circumstances permit.

Extensions of this work to the case of the planar array are treated briefly in Appendix A.

SECTION VII

DISCUSSION OF RESULTS AND CONCLUSIONS

This work represents a different approach to the design of discrete arrays. The subject area has been intensively pursued over the years with outstanding results by many capable investigators. The main value of this particular work lies, perhaps, in the exposition of new points of view on an old problem. Such transients in established thought patterns can quite often produce beneficial effects.

The data shown in Table 4-1 indicates that the design procedure is generally competitive with prior-art approaches in terms of aperture size and efficiency. The procedure is based on discrete arrays from the outset. This eliminates problems that can sometimes arise when continuous distributions are sampled to obtain element weights.

The procedure also lends itself to implementation using interactive computer techniques. This is especially true in the truncation operation described in Section V. In many cases the reference arrays obtained directly from the interpolator cascade have extended sidelobe areas of very-low level. Truncation tends to fill these regions back up in exchange for a smaller aperture and higher efficiency. In some cases a larger than minimum aperture and a lower than maximum efficiency may be readily accepted in exchange for extra sidelobe suppression in extended regions. Interactive computer operation usage of these procedures can be most helpful in tailoring an array design to a specific practical application.

It also appears that the freedom given to the array in terms of sidelobe variation (only the peak value is directly manipulated by the design) may contribute to the well-behaved nature of the current distributions which result. It is the nature of this procedure that current distributions will always taper smoothly to zero at the aperture edges regardless of the beamwidth or sidelobe specification imposed. A minor advantage of the technique may lie in the fact that weight calculations for any pattern specification are straightforward almost to the point of being trivial.

The feed matrix and aperture combination developed in Section VI has the immediate advantage of novelty. Conventional beam steering employs no amplitude control, but provides individual phase adjustment for each element. The system of Section VI uses one phase shifter but requires level (and polarity) control at each element. For constant-envelope waveforms, the phase shifter approach is a compatible one. If more general types of signal waveforms are to be handled, then the options will have to be reexamined. At the least, the beamforming system of Section VI gives to the designer one more option from which to make a selection.

The basic concept demonstrated in Section VI involves the use of interpolation techniques to generate currents for use in a displaced element set to match the far-field pattern of an original element set. The specific use made of this concept permitted separation of in-phase and quadrature current radiators in an array. However, this certainly does not exhaust the possible uses of the basic concept demonstrated.

SECTION VIII

REFERENCES

[1] J. P. Costas, "An Iterative Interpolation Technique Using Finite Impulse Response Digital Filters," General Electric Company Technical Information Series Report No. R79EMH1, February, 1979.

[2] L. R. Rabiner and B. Gold, "Theory and Applications of Digital Signal Processing", Prentiss-Hall, Englewood Cliffs, N.J., 1975.

[3] C. L. Dolph, "A Current Distribution for Broadside Arrays Which Optimizes The Relationship Between Beamwidth and Sidelobe Level," Proc. I. R. E., Vol 34, pp. 335-348; June 1946.

[4] H. F. Riblet, Discussion on "A Current Distribution for Broadside Arrays Which Optimizes the Relationship Between Beamwidth and Sidelobe Level", Proc. I. R. E., Vol 35, pp 489-492; May, 1947.

APPENDIX A

EXTENSION OF ARRAY SUBSTITUTION PROCEDURES TO TWO DIMENSIONS

The array substitution procedures of Section VI will be extended to cover the planar array case in the following. Figure A-1(b) shows the coordinate system chosen here for the discussion. The far-field point E lies at a distance ρ from the origin with azimuth angle θ and elevation angle ϕ. The array is assumed to be in the y-z plane with element spacing T as shown in Figure A-1(a). Let the array be in the first quadrant of the y-z plane and let an element location be specified by its (y, z) coordinates.

If d is defined as the distance from the element to the far-field point, E, some simple geometry yields, for $\rho \rightarrow \infty$

$$\rho - d = y \cos \phi \sin \theta + z \sin \phi \tag{A-1}$$

The phase advance due to distance of an element at (y, z) relative to an element at the origin is

$$\phi_a = \frac{2\pi}{\lambda} (y \cos \phi \sin \theta + z \sin \phi) \tag{A-2}$$

Consider now an element of the original array W_{jk} which, for convenience, will be normalized to unit current. It is also convenient to consider the coordinate system origin to be relocated to the W_{jk} location. It is now desired that the far-field pattern of the unit current W_{jk} be duplicated as closely as possible by a substitution element set g_{jk} in the W_{jk} neighborhood. If the phase of the substitution element set far-field pattern is required to match the phase of the W_{jk} radiation at all far-field points, the g_{jk} must be chosen in groups of four with each member of the group (quad) driven by the same current; that is, for every first quadrant element at (y, z) (relative to W_{jk}), one needs three additional elements at (-y, z), (-y, -z), and (y, -z) all driven with the same current, I_{jk}.

With y and z measured from W_{jk}, the far-field pattern of any such quad will be

$$E_{jk}(\theta, \phi) = 2I_{jk} \left\{ \cos \left[\frac{2\pi}{\lambda} (y \cos \phi \sin \theta + z \sin \phi) \right] + \cos \left[\frac{2\pi}{\lambda} (-y \cos \phi \sin \theta + z \sin \phi) \right] \right\} \tag{A-3}$$

where y and z are the coordinates of the first-quadrant element and I_{jk} is the common current drive to the four substitution elements.

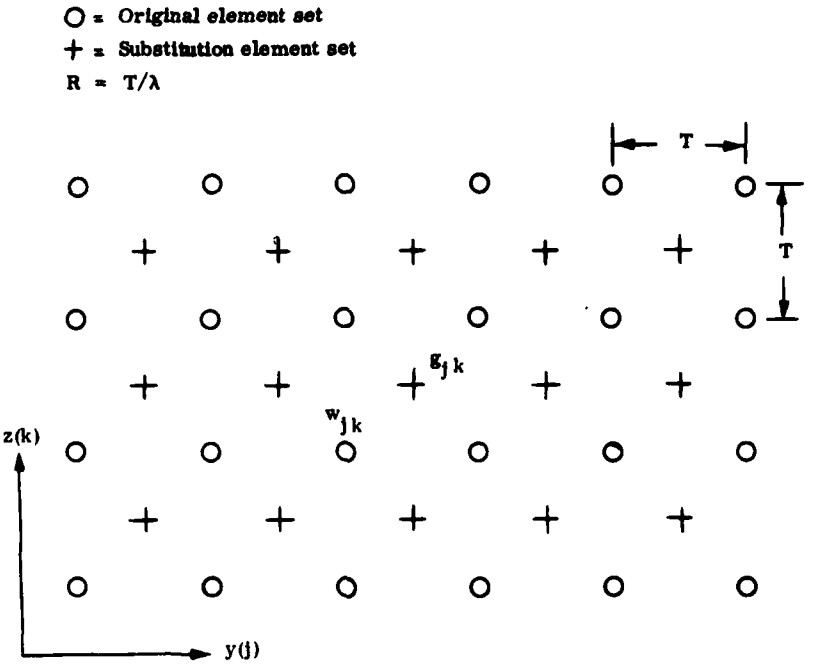

(a) Planar Array Geometry

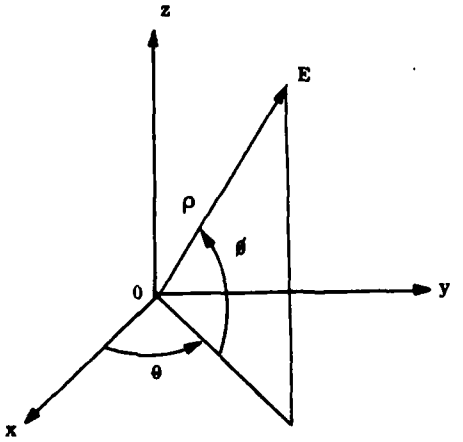

(b) Coordinate System

Figure A-1. Planar Array Description

Define

$$f \triangleq \sin\theta \tag{A-4}$$

$$g \triangleq \sin\phi \tag{A-5}$$

$$b_r \triangleq 2\,a_r \tag{A-6}$$

and let (Figure A-1(a))

$$y = (2j-1)\,\frac{T}{2} \tag{A-7}$$

$$z = (2k-1)\,\frac{T}{2} \tag{A-8}$$

and require that

$$I_{jk} = a_j\,a_k \ . \tag{A-9}$$

Equation (A-3) may now be rewritten as

$$E_{jk}(f,g) = b_j\,b_k \cos\left[\frac{\pi}{R}(2j-1)\sqrt{1-g^2}\,f\right] \times \cos\left[\frac{\pi}{R}(2k-1)\,g\right] \ . \tag{A-10}$$

This equation gives the far-field contribution of four particular elements which are symmetrically located about W_{jk}, and identified by the row, column coordinates of the first quadrant member of the quad. If N rows of g_{jk} elements above and below W_{jk} are to be used in the substitution process along with N columns to the right and left of W_{jk}, then the total far-field pattern of the substitute array for W_{jk} will be

$$E(f,g) = \sum_{j=1}^{N}\sum_{k=1}^{N} E_{jk}(f,g)$$

$$= \sum_{j=1}^{N} b_j \cos\left[\frac{\pi}{R}(2j-1)\sqrt{1-g^2}\,f\right] \sum_{k=1}^{} \rangle_k \cos\left[\frac{\pi}{R}(2k-1)g\right]$$

so that

$$E(f,g) = H\left(f\sqrt{1-g^2}\right) H(g) \tag{A-11}$$

where H (f) is the ubiquitous function defined in Equation (1-3). It is useful to consider Equation (A-11) to be an effective element pattern of the substitution element set whose array factor is obviously the same as that of the original element set. It then follows that the far-field pattern of the substitution element set is that of the original array times the E (f, g) function of Equation (A-11).

It should be recalled that in the above development a particular excitation procedure was involved for a set of substitution elements in the neighborhood of an original element in an attempt to duplicate the far-field function of that original element. Equation (A-11) shows that the substitute far-field pattern matches the original without error in phase. The error in level is controlled by the H function product of Equation (A-11.) In the x-y plane, $\phi = 0$, $g = 0$ and

$$E(f,0) = H(0)\, H(f) \qquad \text{(A-12)}$$

In the x-z plane, $\theta = 0$, $f = 0$ and

$$E(0,g) = H(0)\, H(g) \qquad \text{(A-13)}$$

Since $H(0) \cong 1$, *the behavior in these principal planes is similar* to that of the line array as discussed in Section VI. For a given N value and corresponding a_n set of Equation (1-3), the behavior of H (f) is known. Therefore, Equation (A-11) may be used to determine the performance level of the substitution array for any f, g combination.

Steering of the planar array will require complex element currents. If desired, the real components may be kept in the original array and the complex components may be placed in the substitution element set as was done for the line array of Section VII to avoid the need for phase shifters. Once the relationship of Equation (A-11) is established, the equivalences between the line and planar array are so close as to make elaboration superfluous.

Equation (A-9) was based on a unit current in the element W_{jk} for which the substitution was being done. The indices j, k were a measure of the y-and z-distances from W_{jk} as is clear from Equations (A-7) and (A-8). If one considers the total current in g_{jk} resulting from substitution operations targeted at a group of original elements W_{jk} in the g_{jk} neighborhood, there results

$$g_{jk} = \sum_{q=1}^{N} a_q \left\{ \sum_{r=1}^{N} \left(a_r W_{j-r+1,\, k+q} + a_r W_{j+r,\, k+q} \right) \right.$$

$$\left. + \sum_{r=1}^{N} \left(a_r W_{j-r+1,\, k-q+1} + a_r W_{j+r,\, k-q+1} \right) \right\} . \qquad \text{(A-14)}$$

This is a double interpolation process. The first interior sum on r represents an interpolation to obtain intermediate element currents in the rows above g_{jk} (compare Equations (2-9) and (A-14)). The second interior sum on r obtains the intermediate element currents in the rows below g_{jk}. The outer sum over q in Equation (A-14) represents an interpolation operation on the intermediate row values in order to obtain the intermediate column values which are the actual substitution element currents g_{jk}. It follows that Equation (A-14) defines an efficient feed matrix algorithm.

APPENDIX B

A SWITCHABLE END-FIRE ELEMENT FOR USE IN THREE-DIMENSIONAL ARRAYS

A particular extension of the work of Section III is presented here. The array of Figure 3-1 is redrawn in Figure B-1(a) while the far-field pattern of Figure 2-1(e) is shown for convenience in Figure B-1(b). The array of Figure B-1(a) has a pattern which is very nearly uniform out to $f = \gamma R/4$ and is close to zero beyond $f = (2-\gamma) R/4$. We have here an unusual result as discussed in Section IV relative to Figures 4-9 and 4-10. A far-field pattern has been produced in Figure B-1(b) which has a uniform gain over an extended region in the mainlobe and a controlled-level stop band in the sidelobe region. This unusual characteristic will now be put to good use.

Let the array of Figure B-1(a) be steered to $f_0 = R/4$ so that the pattern of Figure B-1(c) results. Now define visible space by placing $\theta = \pm \pi/2$ at $f = \pm (1+\gamma) R/4$. This forces an R value of

$$R = 4/(1+\gamma) \tag{B-1}$$

and an element spacing parameter of

$$T = \lambda/R = (1+\gamma)\, \lambda/4 \tag{B-2}$$

This places the center of the main beam at $\theta = +90°$. As θ decreases the gain remains nearly uniform until the start of the transition region at

$$\theta_t = \sin^{-1}\left[(1-\gamma)\, \frac{R}{4} \right] = \sin^{-1}\left[\frac{(1-\gamma)}{(1+\gamma)} \right] \tag{B-3}$$

is encountered. The center of the transition region is at broadside ($\theta = 0°$) and the array gain is -6 dB here. The stop band region beings at $\theta = -\theta_t$ and continues to $\theta = -90°$.

Consider now a planar array having line arrays of the above type as elements with the axis of the lines normal to the plane. The resulting three-dimensional array does not require a backscreen as the element pattern properties provide this function automatically. In fact, a polarity change of the excitation of the center element of Figure B-1(a) will reverse the element pattern so that the main beam appears at $\theta = -90°$. Thus a transparent planar array can cover two sectors. The axial symmetry of the line array element pattern permits planar array steering in both azimuth and elevation. Because of reduction in effective aperture as the planar array is steered toward planar end fire (which is at $\theta = 0$ in Figure B-1(c), the scan angle will probably be limited by this factor. This eases the line element design as will be seen. As a practical matter it would appear that a pair of orthogonal vertical planes could

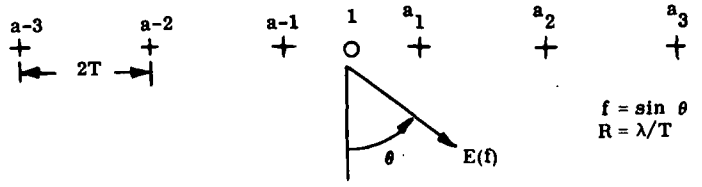

a) Array Geometry

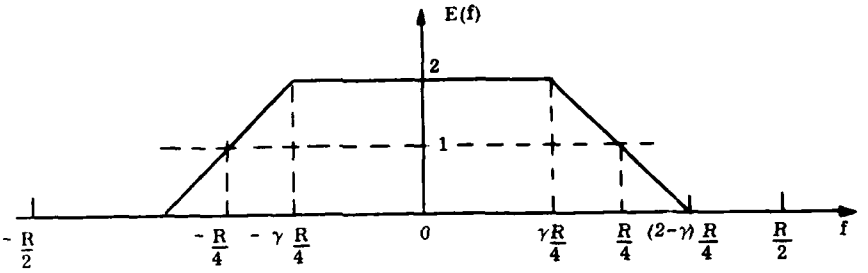

b) Unsteered Array Pattern

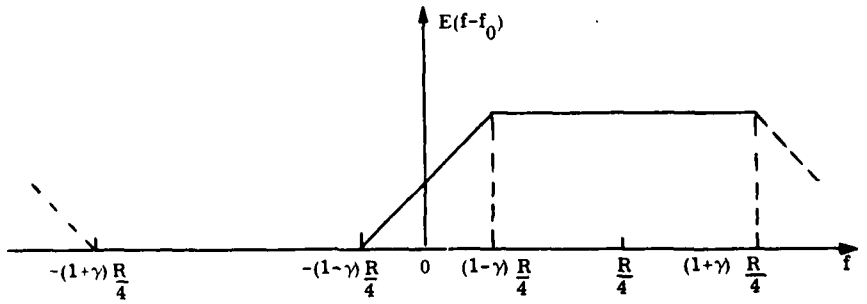

c) Pattern for Steering to $f_0 = R/4$

Figure B-1. End-Fire Array Element Details

easily provide full azimuthal and reasonable elevation coverage. A third horizontal plane would give full spherical coverage.

The phase taper required for steering the line array to $f_0 = R/4$ is given by the weight multipliers w_k

$$w_k = e^{-j2\pi k \frac{f_0}{R}} = e^{-j\frac{\pi}{2}k} \qquad \text{(B-4)}$$

where the index k is now referenced to the array end with w_1 relating to the element at the left end of Figure B-1(a). Since R is based on the spacing T, and since all of the even-index elements are missing except for the center element, all of the element currents are pure imaginary except for the center current which is entirely real. The current distribution shows an odd symmetry about the center element. Quite obviously one can shift the phase of each current by 90° so that all currents become real except for the center one which now becomes imaginary. Also note from Equation (B-4) that steering to $f_0 = -R/4$ may be accomplished by changing the center-element excitation from +1 to -1. The bi-phase philosophy proposed in Section VI for main-array steering can apparently provide a useful function at the element level also.

Some examples of end-fire array designs are shown in Figures B-2, B-3 and B-4. In Figure B-2 a γ value of 0.3 was used which required a T value of 0.325λ. The transition angle θ_t is 33° which would allow a main-array scan angle of ±57° from broadside on each of the two planar faces. This design would be suitable for a main pattern sidelobe specification of about -55 dB. If higher sidelobe levels are involved a simpler end-fire design results. For example the 5 active elements involved in the array of Figure B-2 may be reduced to 3 for a -30 dB sidelobe level for the same scan angle.

Figure B-3 shows a nominal -30 dB design for $\gamma = 0.6$ which reduces the transition angle to 15° permitting scanning to ±75°. The number of active elements is still five which indicates that sidelobe level was traded for increased scan angle for a fixed end-fire element complexity.

This technique can easily be pushed to impractical limits as shown in Figure B-4. Here $\gamma = 0.9$ which yields a transition angle of 3° and a scan angle of ±87°. This end-fire design required 39-active elements to achieve the scan angle and sidelobe performance shown. It turns out that sidelobe level is not nearly as expensive as is scan angle as regards active element count. This is fortunate since loss of effective aperture will limit the scan angle in most practical designs. At the scan angles anticipated, the end-fire element designs appear to be quite manageable.

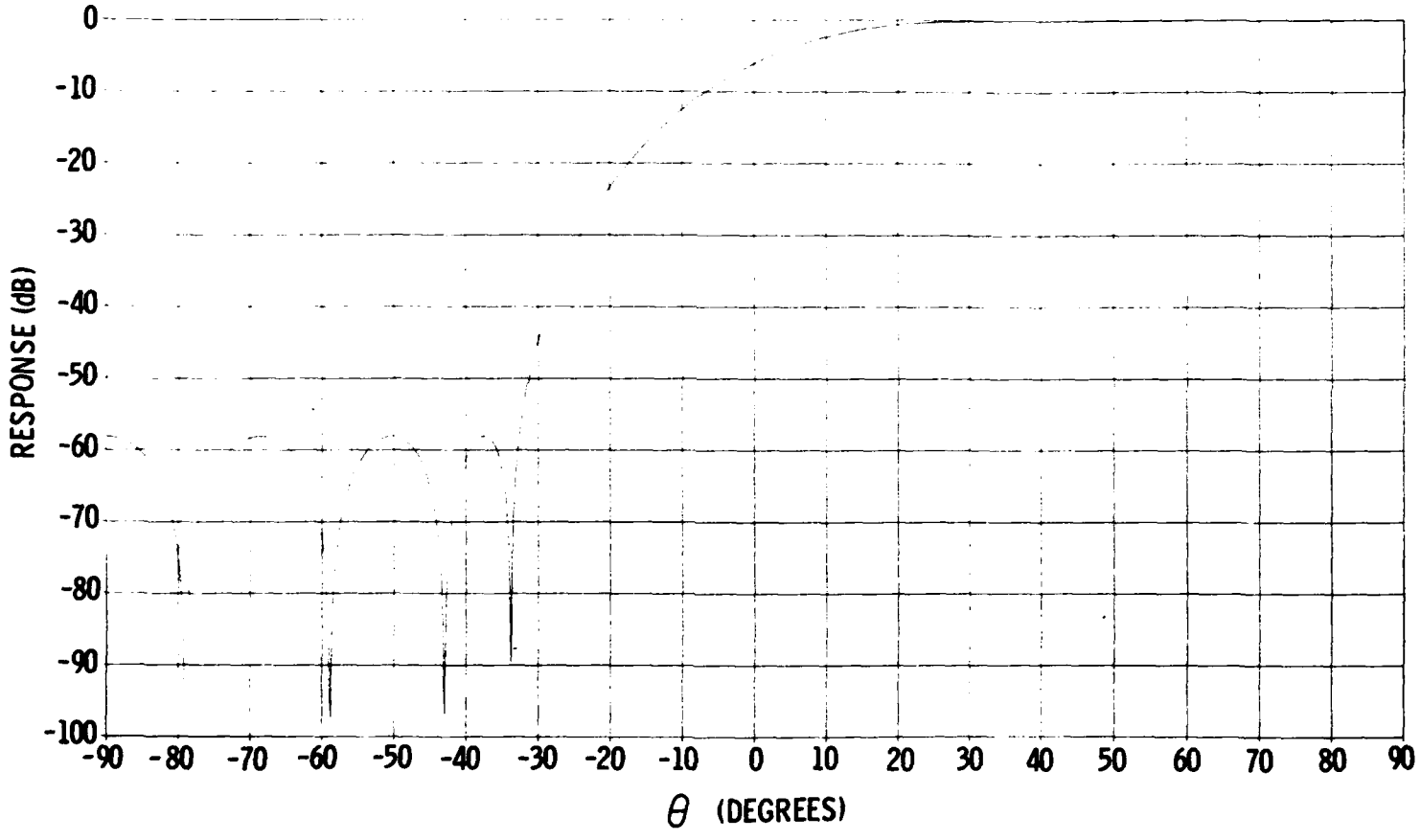

Figure B-2. Line Array Pattern, 5 Active Elements, ($\gamma = 0.3$, $T = 0.325\lambda$, Scan Angle = ±57°)

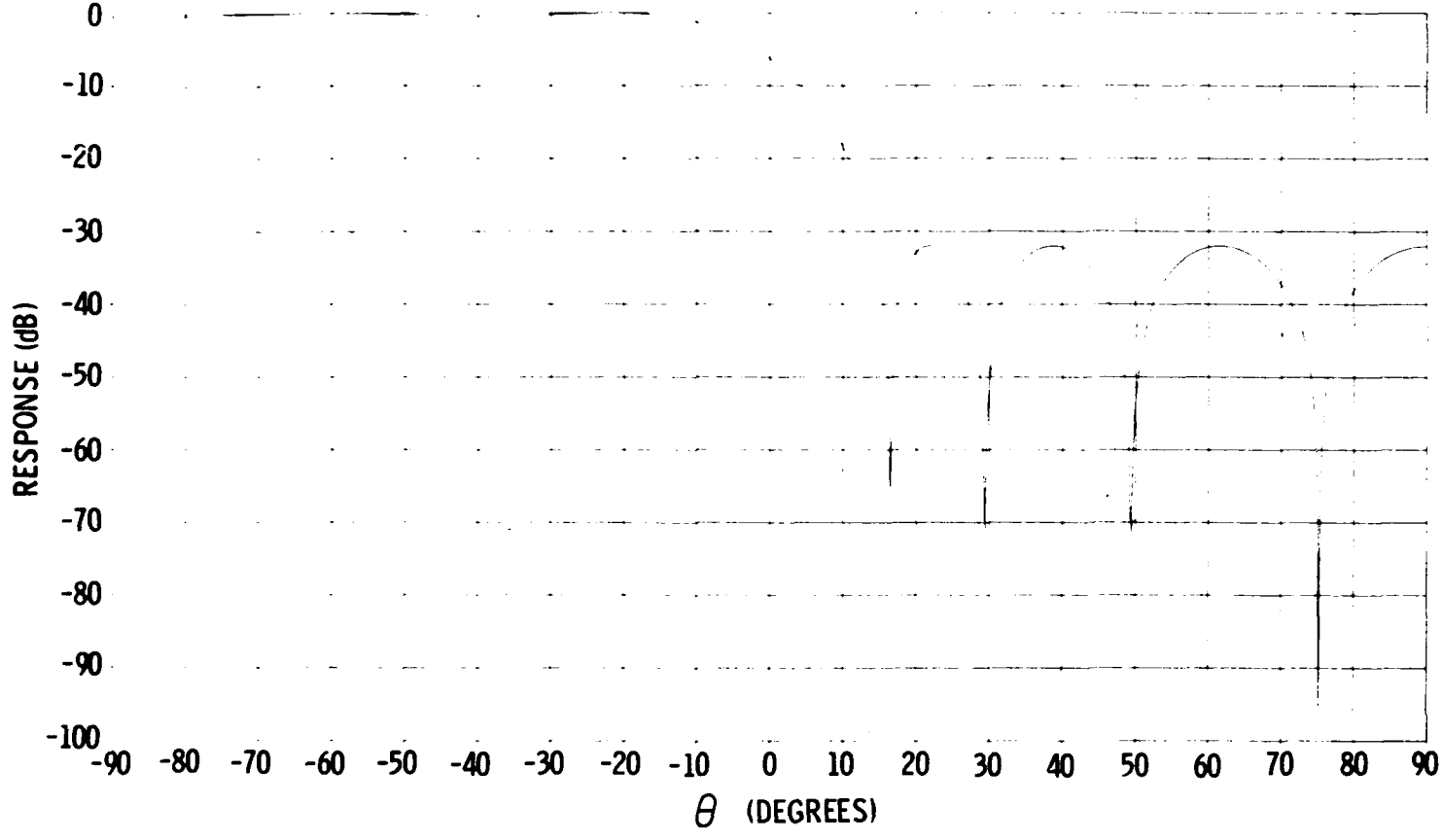

Figure B-3. Line Array Pattern, 5 Active Elements,($\gamma = 0.6$, $T = 0.40\lambda$, Scan Angle = ±75°)

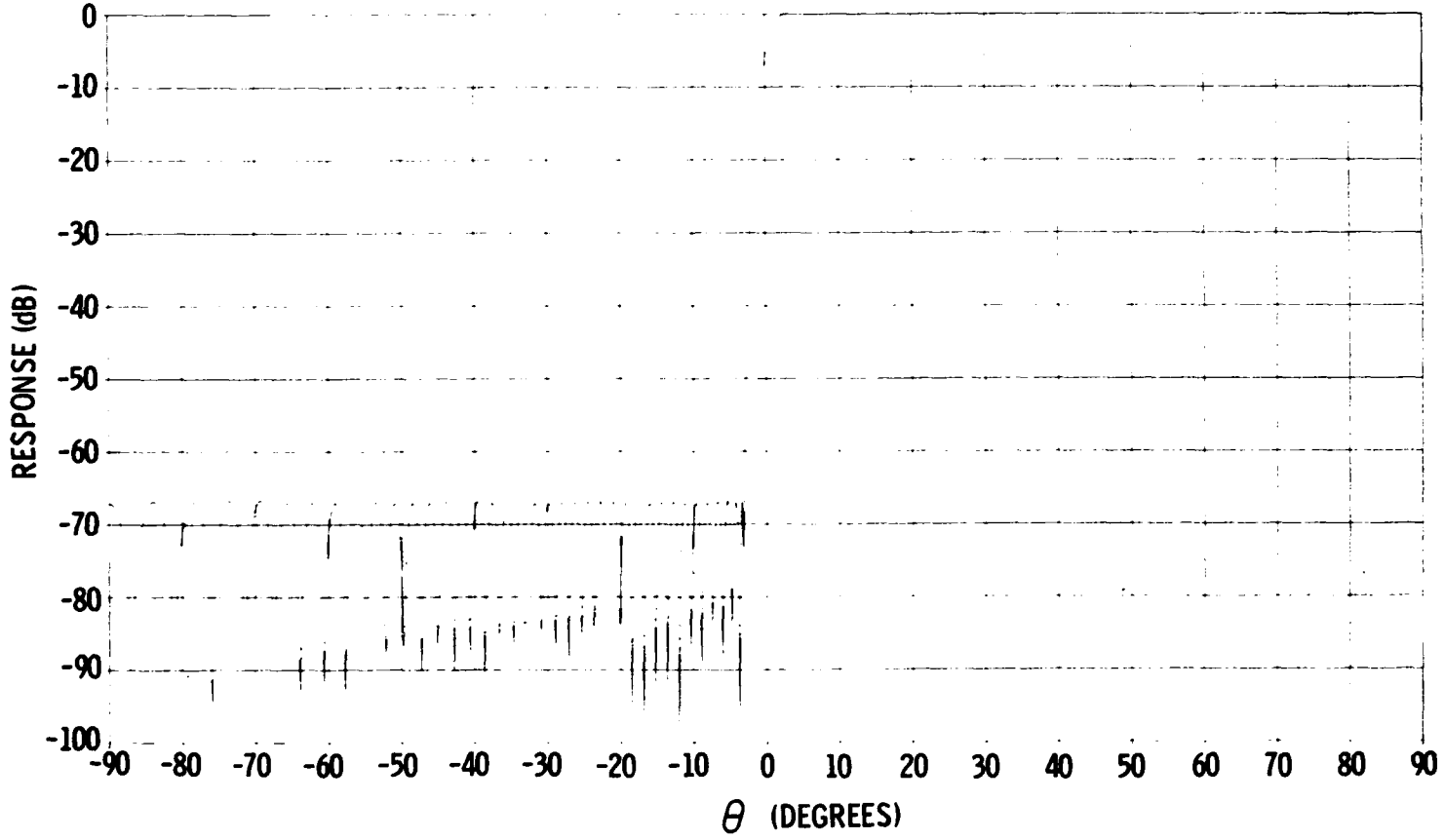

Figure B-4. Line Array Pattern, 39 Active Elements, ($\gamma = 0.9$, T = 0.475λ, Scan Angle = ±87°)

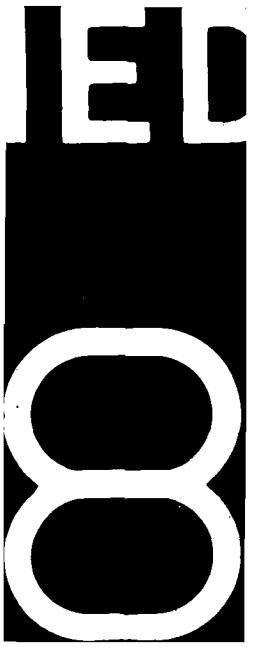
ED
8